Thermal-difference reflectance spectroscopy of the high-temperature cuprate superconductors

M. J. Holcomb and C. L. Perry
Department of Chemistry and Department of Physics, Stanford University, Stanford, California 94305

J. P. Collman
Department of Chemistry, Stanford University, Stanford, California 94305

W. A. Little
Department of Physics, Stanford University, Stanford, California 94305

(Received 28 July 1995)

The temperature-dependent thermal-difference reflectance (TDR) spectra of thin-film samples of $Tl_2Ba_2Ca_2Cu_3O_{10}$, $(BiPb)_2Sr_2Ca_2Cu_3O_{10}$, $Tl_2Ba_2CaCu_2O_8$, and $YBa_2Cu_3O_7$ have been measured for photon energies between 0.3 and 4.5 eV at temperatures above and below each material's superconducting critical temperature. The amplitude of the characteristic optical structure near the screened plasma frequency of each sample in the normal-state TDR spectrum varies approximately linearly with temperature, T, indicating that the temperature-dependent optical scattering rate in these materials scales with temperature as T^2. From the TDR spectra collected above and below the critical temperature of each sample, the superconducting to normal-state reflectance ratio, R_S/R_N, has been obtained. In all of these spectra, there are significant deviations from unity in R_S/R_N at photon energies on the order of 2.0 eV. This optical structure cannot be accounted for using the conventional Mattis-Bardeen description of the optical properties of a superconductor or its strong-coupling extension where electron-pairing interactions are limited to energies less than 0.1 eV. However, both the temperature and energy dependence of the structure in the R_S/R_N spectra may be adequately described within Eliashberg theory with an electron-boson coupling function which consists of both a low-energy component ($<$0.1 eV) and a high-energy component located between 1.6 and 2.1 eV.

I. INTRODUCTION

Common to most theories of high-temperature superconductivity is the assumption of an underlying mechanism by which the electrons pair at the superconducting critical temperature, T_c. From this assumption, it follows that there is a unique electron pairing potential, Δ, associated with each mechanism and that the energy and momentum dependence of this pairing potential, $\Delta(\omega,\mathbf{k})$, will reflect the microscopic origin of the pairing interaction. Historically, these ideas parallel Eliashberg's extension[1] of the BCS model of superconductivity[2] which took into account the retarded nature of the electron-phonon interaction. In an isotropic model, the Eliashberg electron-pairing potential, or superconducting gap function, is a complex energy and temperature-dependent function, $\Delta(\omega,T)$, whose structure reflects the underlying energy-dependent electron-phonon interaction.[3] Experimentally, $\Delta(\omega,T)$ may be obtained through high precision measurements of the conductance versus bias voltage of a normal/insulator/superconductor ($N/I/S$) tunnel junction, and from these data, the energy-dependent electron-boson coupling spectrum, $G(\omega)$, may be calculated through an inversion of the Eliashberg integral equations.[4] In materials where the superconductivity is solely mediated through the electron-phonon interaction, $G(\omega)$ is more precisely written as $\alpha^2(\omega)F(\omega)$ where $\alpha^2(\omega)$ is the square of the electron-phonon matrix element and $F(\omega)$ is the phonon density of states. The spectral form of $G(\omega)$ obtained from tunneling experiments, and its similarity to the measured phonon density of states in low-T_c superconductors, provided incontrovertible proof that the effective attractive interaction provided by the electron-phonon interaction was both necessary and sufficient to account for the superconductivity in these materials.

In principle, once the underlying electron-boson coupling function is determined with sufficient accuracy, any property of the superconducting state may be calculated. Thus, internal consistency between experiments which probe different properties of the superconducting state may be achieved by interpreting these measurements using the $G(\omega)$ obtained from tunneling data. On the other hand, measurements of the temperature dependence of the NMR relaxation rate,[5] the thermodynamic critical magnetic field,[6] the London penetration depth,[7] and the electronic specific heat[8] in the superconducting state, for example, do not measure the energy dependence of $\Delta(\omega,T)$ and thus do not contain detailed information about the microscopic nature of the underlying electron-pairing interaction. Instead, these measurements represent quantities which may be calculated through an integration over energy, where the integral contains the energy dependent $\Delta(\omega,T)$. When an experiment does not involve the direct measurement of the energy dependence of $\Delta(\omega,T)$, it is only possible to interpret the results as being *consistent* with an assumed microscopic form of the pairing interaction.

Although the many different experiments which probe the superconductivity in the high-T_c cuprate superconductors give some insight into the mechanism of superconductivity, it is only those experiments which probe the excitation spectrum of these materials in the superconducting state which can provide detailed insight into the microscopic nature of

the electron-pairing interaction. Some of the more common experimental methods which can, in principle, measure $\Delta(\omega,\mathbf{k},T)$ are $N/I/S$ tunneling, angle-resolved photoelectron spectroscopy (ARPES), Raman spectroscopy, and conventional optical spectroscopy (i.e., reflectance and transmittance).

Tunneling measurements are, by far, the most common means of determining the energy dependence of the pairing potential in a superconductor. The conductance versus bias voltage of an $N/I/S$ junction at sufficiently low temperatures is directly proportional to the superconducting density of states, $N_S(\omega)$, given by[3,4,9]

$$N_S(\omega)=N_N(\omega)\mathrm{Re}\left(\frac{\omega}{\sqrt{\omega^2-\Delta^2(\omega)}}\right), \tag{1}$$

where $N_N(\omega)$ is the normal-state density of states. From the form of Eq. (1), it is seen that the presence of a finite $\Delta(\omega)$ at temperatures less than T_c modifies the normal-state density of states in the material. For energies less than the gap edge, Δ_0, defined as the magnitude of the real part of $\Delta(\omega)$ evaluated at energy ω equal to the real part of $\Delta(\omega)$ at energy $\omega\sim 0$, $N_S(\omega)$ is zero. At energies greater than Δ_0, the energy-dependent structure of $\Delta(\omega)$ manifests itself as small modulations in the tunneling conductance at energies corresponding to peaks in $G(\omega)$. Conductance data are usually normalized by dividing $N_S(\omega)$ by $N_N(\omega)$. $\Delta(\omega)$ may then be obtained from the normalized conductance and from this, the Eliashberg integral equations may be inverted to obtain $G(\omega)$.[4,10] Implicit to Eq. (1) is an average over the Fermi surface leaving an expression which is only a function of energy ω.

Unfortunately, there are significant problems involved in making adequate tunneling junctions with the cuprate superconductors. Since the amplitude of the tunneling current varies as $\exp\{-d/\xi\}$, where d is the thickness of the tunneling barrier, and since the cuprate superconductors have naturally short coherence lengths, $\xi\sim 15$ Å, the tunnel barrier must be thin and of uniform thickness over the junction area. These requirements are made more difficult to attain given the natural surface reactivity of these materials. In recent years, the techniques for making good tunneling junctions with these materials, particularly the bismuth-based cuprate superconductors, have improved dramatically and high-quality conductance spectra have been obtained.[11–14] In general, these data have been inverted using the McMillan/Rowell inversion procedure.[4] The results of this inversion indicate that there is significant electron-phonon coupling in these materials. Evidence for this is obtained from the similarity between the phonon density of states in the materials measured by inelastic neutron scattering[15–18] to the $G(\omega)$ obtained through the inversion of the conductance data. This is exactly the line of reasoning which resulted in the determination that superconductivity was the result of the electron-phonon interaction in low-temperature superconductors. The calculated $G(\omega)$ is not, in general, sufficient to account for the high-T_c of the materials with critical temperatures greater than approximately 50 K. The higher critical temperatures, on the other hand, may result from a high density of electronic states near the Fermi level, due to the presence of a Van Hove singularity, for example, or an additional high-energy component of the electron pairing interaction which is not sampled by the tunneling spectrum.[19] The latter represents a fundamental limit of tunneling spectroscopy, that is, it is only possible to extract $G(\omega)$ from conductance data up to the maximum bias voltage of the tunneling junction set by its voltage breakdown limit. In typical tunneling junctions, this maximum is of the order of 100 meV.

A potentially promising method of determining both the energy and momentum dependence of the superconducting gap function, $\Delta(\omega,\mathbf{k})$, is angle-resolved photoelectron spectroscopy (ARPES). This technique measures the energy and momentum dependence of the one-particle spectral function, $A(\omega,\mathbf{k})$.[20] This quantity is related to the superconducting density of states as a function of both energy and crystal momentum, $N_S(\omega,\mathbf{k})$, and thus is a direct measurement of $\Delta(\omega,\mathbf{k})$. A fundamental limitation of this method is that it only probes the surface ($\sim$20 Å) of the material. Consequently, the best data have been obtained on $Bi_2Sr_2CaCu_2O_8$ single crystals which are known to have one of the least reactive surfaces of the cuprate superconductors and which cleave easily in vacuum. Analogous to tunneling experiments, information about $\Delta(\omega,\mathbf{k})$ is obtained from small modulations in $A(\omega,\mathbf{k})$ at energies well above Δ_0. Typically these modulations are of order $\{\Delta(\omega)/\omega\}^2$ which may only be a fraction of a percent of the total measured quantity. This places a restriction on the tolerable signal-to-noise ratio (SNR) at $\sim 10^5$ if $G(\omega,\mathbf{k})$ is to be extracted from these measurements. At present, this SNR cannot be achieved with modern experimental techniques, thus no information on $G(\omega,\mathbf{k})$ can be obtained with ARPES.

Despite this, ARPES experiments have provided important information concerning the symmetry of the superconducting gap edge, $\Delta_0(\mathbf{k},T)$. The magnitude of $\Delta_0(\mathbf{k},T)$ is obtained in ARPES by fitting the energy distribution curves measured along specific symmetry directions to a phenomenologically broadened BCS spectral function.[21–23] The results indicate significant anisotropies exist in the magnitude of the gap edge with momentum and that $\Delta_0(\mathbf{k},T)$ is large in the $\Gamma-M$ direction, along the Cu-O bond, and close to zero on either side of the (π,π) directions. Unfortunately, because the technique measures only $|\Delta_0(\mathbf{k},T)|$, it is not possible to determine if $\Delta_0(\mathbf{k},T)$ changes sign as a function of $\mathbf{k}$. These measurements provide direct evidence that the superconducting gap function in these materials is highly anisotropic, which is not surprising given their structural anisotropy.

Similarly, Raman spectroscopy has been used to probe the symmetry of the superconducting gap edge.[24–30] The polarization dependence of the electronic Raman spectra of the cuprate superconductors yields information about the underlying symmetry of $\Delta_0(\mathbf{k},T)$. By fitting the measured spectra with model systems based upon BCS-like superconducting gaps of various symmetries, conclusions about the symmetry of $\Delta_0(\mathbf{k},T)$ can be drawn.[31] Like ARPES, these measurements suggest that there is significant anisotropy of the superconducting gap in these materials, they cannot, however, distinguish between a true $d_{x^2-y^2}$ superconducting gap and a highly anisotropic s-wave gap[27,31–33] as it is only possible to extract the magnitude of $|\Delta_0(\mathbf{k},T)|$, and not the sign of $\Delta_0(\mathbf{k},T)$, from the spectrum. Even though electronic Raman spectroscopy is a powerful technique for probing the symmetry of $|\Delta_0(\mathbf{k},T)|$, its use appears limited in the determina-

tion of $\Delta(\omega,\mathbf{k},T)$ because of experimental problems associated with correcting for the energy-dependent optical constants of the material, the removal of the phonon structure in the spectra, and the relatively low SNR as compared to tunneling measurements.

A powerful, but perhaps underutilized experimental technique available for use in the determination of the energy and momentum dependence of $\Delta(\omega,\mathbf{k},T)$ is optical spectroscopy. The transmittance or reflectance spectrum of a superconductor is a measure of both a superconducting joint density of states and a joint case II coherence factor function.[34,35] Thus, the reflectance or transmittance spectrum of a superconductor is, in principle, a direct measurement of $N_S(\omega,\mathbf{k})$, and thus is a direct measurement of $\Delta(\omega,\mathbf{k})$. Unfortunately, this measurement suffers all of SNR constraints imposed by the small magnitude of $\Delta(\omega,\mathbf{k})$ with respect to the excitation energy. In addition, the inversion of optical data is complicated by the existence of case II coherence factors which enter into the standard expressions describing the operative optical-absorption process of a superconductor. Like $N/I/S$ tunneling, this approach has a long history in the study of conventional low-temperature superconductors,[36–42] but because of the inferior signal-to-noise ratios in these measurements as compared to tunneling measurements and the numerical complexity of the inversion process, no rigorous inversion of optical data has been attempted.

The optical properties of the cuprate superconductors have been measured by many laboratories.[43–59] Often, these measurements extend well into the superconducting state, and in general, these measurements concentrate on the existence of the optical gap edge, $2\Delta_0(T)$, even though it is well known that it is the small variations in the optical properties of a superconductor at energies well above $2\Delta_0(T)$ that contain information on the nature of the pairing interaction.

The important quantity measured in an optical experiment performed on the high-T_c superconductors is the superconducting to normal-state reflectance ratio, R_S/R_N, or the ratio of the real part of the optical conductivity in the superconducting state to that in the normal state, $\mathrm{Re}\{\sigma_S(\omega)\}/\mathrm{Re}\{\sigma_N(\omega)\}$. Unlike R_S/R_N which can be measured directly, the conductivity ratio is usually calculated with the help of the Kramers-Kronig relations. Unfortunately, systematic uncertainties in the Kramers-Kronig transformation limit the precision of the measurement such that the minute structure resulting from the energy dependence of the gap function is lost at energies well above the optical gap edge.

Reflectance measurements, on the other hand, are ideally suited as a means of obtaining information about $G(\omega)$ operative in the cuprate superconductors. Most importantly, the reflectance R is a quantity that is measured directly. Thus, the precision of the measurement is only a function of the SNR of the instrument used to collect the data. Further, because the light penetrates the sample on the order of 1000 Å,[54] the reflectance measurement probes the bulk superconducting properties of the material. In addition, since it is an optical measurement, it is not limited to energies commonly available to tunnel junctions, thus the properties of the material can be measured over a very wide energy range. Finally, by measuring the reflectance ratio with polarized light, it is possible to obtain information on both the energy and momentum dependence of the superconducting gap function.

In this paper, we report high precision R_S/R_N measurements obtained on a variety of high-temperature cuprate superconductors.[60] The reflectance ratio is obtained by measuring each material's temperature-dependent thermal difference reflectance spectra at temperatures above and below the superconducting critical temperature. We analyze these data using the strong-coupling extension of Mattis-Bardeen[61] theory developed by Nam.[34] We describe the numerical methods employed to fit these data using an iterative procedure which includes solving the finite temperature Eliashberg equations and using the resulting $\Delta(\omega,T)$ to calculate the scattering time in the superconducting state $\tau_S(\omega,T)$ based upon a knowledge of the normal-state scattering time, $\tau_N(\omega,T)$. We discuss the implications of these results and their effect on the possible theories of high-temperature superconductivity.

The paper is divided into four sections. In Sec. II we describe the operation and performance characteristics of the thermal-difference reflectance spectrometer designed to collect these data. Section III develops a framework for the thermal-difference reflectance spectra within the Drude model and shows these data obtained with the spectrometer on a variety of cuprate superconductors in the normal and superconducting state. The formalism within which these spectra are interpreted is described in Sec. IV. We then discuss the conclusions which can be drawn from these results in Sec. V.

II. EXPERIMENTAL

The samples used in this study were high-quality, c-axis-oriented, thin films of $Tl_2Ba_2Ca_2Cu_3O_{10}$ (Tl-2223),[62] $Tl_2Ba_2CaCu_2O_8$ (Tl-2212),[63] $(BiPb)_2Sr_2Ca_2Cu_3O_{10}$ (BiPb-2223),[64] and $YBa_2Cu_3O_7$ (YBCO).[65] The T_c of each sample was determined by the standard four-point probe method, using a low-frequency ($\sim$20 Hz), constant-current amplitude, square wave excitation, and a lock-in amplifier. The T_c of each sample was taken to be the temperature at which the sample's resistance fell to zero within the noise limits of the measurement apparatus ($\sim 10^{-9}$ Ω). The critical temperatures were measured to be $\sim$118 K for Tl-2223, $\sim$106 K for BiPb-2223, $\sim$105 K for Tl-2212, and $\sim$91 K for YBCO.

The optical data were collected with a thermal-difference reflectance (TDR) spectrometer similar to the one described previously.[66] Briefly, a TDR spectrum is obtained by measuring the reflectance spectrum, $R(\omega)$, of a sample at temperature $T_0+\Delta T$, and at $T_0-\Delta T$, then subtracting these quantities and dividing by their average value. Equivalently, the TDR spectrum, $\Delta R_T/R$, is defined as

$$\frac{\Delta R_T}{R}=\frac{R(\omega,T_0+\Delta T)-R(\omega,T_0-\Delta T)}{([R(\omega,T_0+\Delta T)+R(\omega,T_0-\Delta T)/2}$$

$$\approx\frac{[\partial R(\omega,T_0)/\partial T]}{R(\omega,T_0)}\,2\Delta T, \tag{2}$$

where we note that if the changes in the reflectance of the sample are linear within $2\Delta T$, then the TDR spectrum approximates the normalized thermoreflectance[67] of the material. Unless indicated otherwise, we set ΔT equal to 5 K in all of these experiments.

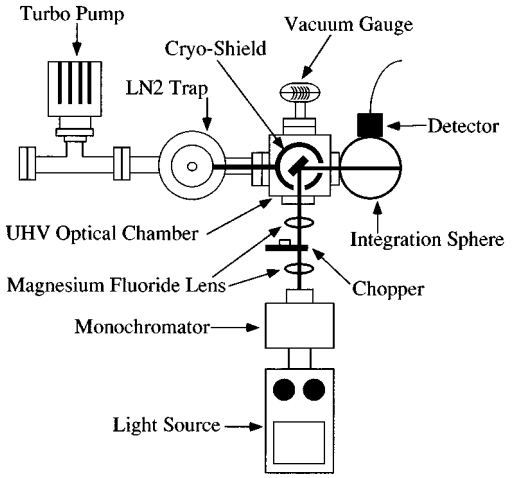

FIG. 1. Schematic diagram of the spectrometer used for thermal difference reflectance measurements of the cuprate superconductors.

A schematic of the TDR spectrometer used in these studies is shown in Fig. 1. The present instrument has an added 77 K cryoshield which surrounds the sample and aids in the collection of high-quality optical data at lower operating temperatures. Each sample was mounted on the cold stage of a small Joule-Thomson refrigerator[68] installed in an ultrahigh-vacuum optical chamber. The refrigerator can maintain the sample temperature between 70 and 350 K with ± 20 mK stability over the course of a scan. The base pressure of the turbo-pumped optical chamber, with the liquid-nitrogen trap filled, was approximately 1×10^{-9} torr. Unpolarized light was incident on the sample at an angle of 45°. The signal from the detector was measured with a digital lock-in amplifier[69] tuned to the optical chopping frequency. With the present optical system, TDR spectra can be collected between photon energies of 0.3 and 5.0 eV.

For each sample, the TDR data were collected continuously for a period of approximately nine days. Each TDR spectrum from 0.3 to 4.5 eV consists of nine different scans. In each scan, the appropriate optics and detectors are chosen to maximize the magnitude of signal measured at the detector, and thus maintain the highest possible SNR over the entire spectrum. Using digital averaging and thermal cycling techniques,[66] the baseline noise of the instrument has been reduced to approximately the one part in 10^5 level. We illustrate this in Fig. 2 where the TDR spectrum of Tl-2212 at 300 K with a $\Delta T=5$ K is shown with the same spectrum collected with a $\Delta T=0$ K. As can be seen, the noise level of the instrument is much smaller than the optical features in the $\Delta T=5$ K TDR spectrum. This extremely low baseline noise allows for the detection of changes in the reflectance of the sample to approximately 0.007%, at photon energies between 0.3 and 4.5 eV, and is thus ideally suited to measure the small changes in the reflectance of a superconductor which may occur upon entering the superconducting state.

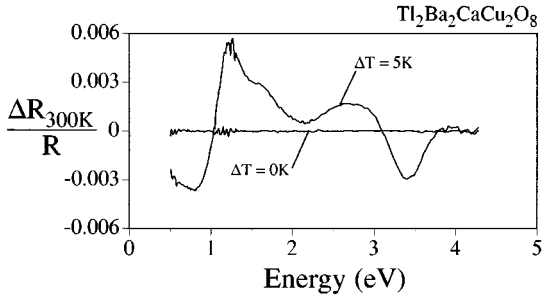

FIG. 2. The thermal-difference reflectance (TDR) spectra of $Tl_2Ba_2CaCu_2O_8$ at 300 K with $\Delta T=0$ K and $\Delta T=5$ K. The data collected with $\Delta T=0$ K establishes the baseline signal-to-noise ratio of the TDR spectrometer at $\sim 7\times10^{-5}$. Thus, by using TDR spectroscopy, it is possible to detect the temperature-dependent changes in a sample's reflectance to ~0.007%.

III. RESULTS

In general, the TDR spectrum of a material is difficult to interpret. Fortunately, however, there are instances in which the derivative line shapes observed in the spectrum are characteristic of a specific optical-absorption process. For example, it is well known that optical absorptions in the derivative spectra of semiconductors display characteristic line shapes which are unique to the nature of the critical points in the joint density of states of the material.[67,70] Also, metals possess a unique derivative line shape whose location corresponds to the energy of the screened plasma frequency of the material.[67] To illustrate typical TDR spectra for metallic materials, we first develop the formalism within Drude theory. After the general features of this type of spectroscopy are shown, we present our TDR spectra of the high-T_c cuprate superconductors.

A. Thermal-difference reflectance spectroscopy in the Drude model

The TDR spectrum of a metal provides information about the temperature-dependent processes which affect the material's optical properties. In the simplest model of the optical properties of a metal, the Drude model, the TDR spectrum arises from the temperature-dependent changes in the material's plasma frequency and scattering rate.[67,70] The optical properties of a Drude metal are determined by three parameters; the bare plasma frequency, the optical scattering rate, and the high-frequency dielectric constant. Given these parameters the reflectance spectrum, R, of a Drude metal at normal incidence is given by[70,71]

$$R=\frac{[\varepsilon_r^2(\omega)+\varepsilon_i^2(\omega)]^{0.5}-\{2\varepsilon_r(\omega)+2[\varepsilon_r^2(\omega)+\varepsilon_i^2(\omega)]^{0.5}\}^{0.5}+1}{[\varepsilon_r^2(\omega)+\varepsilon_i^2(\omega)]^{0.5}+\{2\varepsilon_r(\omega)+2[\varepsilon_r^2(\omega)+\varepsilon_i^2(\omega)]^{0.5}\}^{0.5}+1}, \tag{3}$$

with

$$\varepsilon_r(\omega)=\varepsilon_\infty-\left(\frac{\omega_p^2}{\omega^2+\Gamma^2}\right), \tag{4}$$

and

$$\varepsilon_i(\omega)=\frac{\Gamma}{\omega}\left(\frac{\omega_p^2}{\omega^2+\Gamma^2}\right), \tag{5}$$

where $\varepsilon_r(\omega)$ and $\varepsilon_i(\omega)$ are the real and imaginary components of the complex dielectric function, ε_∞ is the high-frequency dielectric constant, Γ is the Drude scattering rate, and ω_p is the bare plasma frequency given by,

$$\omega_p=\sqrt{\frac{4\pi Ne^2}{m^*}}. \tag{6}$$

In Eq. (6), N is the electron density of the material, m^* is the optical effective mass, and e is the electronic charge. Figure 3(a) shows R for a Drude metal calculated by using Eq. (3) and the Drude model parameters shown in Table I. In this model, the plasma frequency is located at 3.0 eV, the high-frequency dielectric constant is 4.0, and the model is heavily damped with $\Gamma=0.3$ eV. These parameters are similar to those observed in the high-T_c cuprate superconductors. As seen in Fig. 3(a), R is relatively large at low energies and falls abruptly at approximately 1.5 eV near the screened plasma frequency, $\tilde{\omega}_p$, where $\tilde{\omega}_p\sim(\omega_p/\sqrt{\varepsilon_\infty})$. Above $\tilde{\omega}_p$, R passes through a minimum and then increases slowly to a constant magnitude at high energies.

The TDR spectrum of a Drude model is obtained by calculating the partial derivatives of $\varepsilon_r(\omega)$ and $\varepsilon_i(\omega)$ with respect to temperature T, and the partial derivatives of R with respect to both $\varepsilon_r(\omega)$ and $\varepsilon_i(\omega)$. The TDR spectrum may be written as,

$$\frac{\Delta R_T}{R}=\frac{1}{R(\omega,T)}\left(\frac{\partial R(\omega,T)}{\partial\varepsilon_r(\omega,T)}\frac{\partial\varepsilon_r(\omega,T)}{\partial T}+\frac{\partial R(\omega,T)}{\partial\varepsilon_i(\omega,T)}\frac{\partial\varepsilon_i(\omega,T)}{\partial T}\right)2\Delta T, \tag{7}$$

where we now write the temperature and energy dependence of R, ε_r, and ε_i explicitly. The partial derivatives of $R(\omega,T)$ with respect to $\varepsilon_r(\omega,T)$ and $\varepsilon_i(\omega,T)$ may be calculated using Eq. (3) and are independent of the model used to describe the optical properties of the material. The thermal derivatives of the real and imaginary components of the dielectric function, however, are model specific. Within the Drude model, assuming that both the optical effective mass, m^*, and the high-frequency dielectric constant, ϵ_∞, are independent of temperature, these derivatives can be shown to be,

$$\frac{\partial\varepsilon_r(\omega,T)}{\partial T}=\left(\frac{\omega_p^2}{\omega^2+\Gamma^2}\right)\left[\left(\frac{1}{V}\frac{dV}{dT}\right)+\left(\frac{2\Gamma}{\omega^2+\Gamma^2}\right)\frac{d\Gamma}{dT}\right], \tag{8}$$

and

$$\frac{\partial\varepsilon_i(\omega,T)}{\partial T}=\frac{\Gamma}{\omega}\left(-\frac{\partial\varepsilon_r(\omega)}{\partial T}\right)+\left(\frac{1}{\omega}\right)\left(\frac{\omega_p^2}{\omega^2+\Gamma^2}\right)\frac{d\Gamma}{dT}, \tag{9}$$

where V is the unit-cell volume, dV/dT is the derivative of the unit-cell volume with respect to temperature, and $d\Gamma/dT$ is the derivative of the Drude scattering rate with respect to temperature. The parameters V, dV/dT, and Γ are, in general, temperature dependent. The Drude TDR spectrum may then be calculated with Eq. (7) by inserting typical values of V, dV/dT, and $d\Gamma/dT$ into Eqs. (8) and (9). In most metals, the thermal-expansion coefficient, $(1/V)dV/dT$, is approximately 10^{-5} K^{-1}, and $d\Gamma/dT$ is approximately Boltzmann's constant, k_B.[67] Using the Drude parameters in Table I, the TDR spectrum of this model is shown in Fig. 3(b). The spectrum shows a distinctive derivative response at energies close to the screened plasma frequency. In Fig. 3(b), $\tilde{\omega}_p$ is seen to be located at an energy very close to the negative peak in the TDR spectrum.

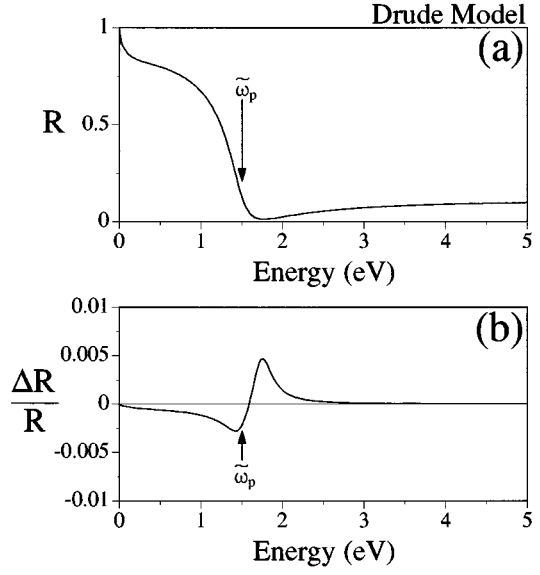

FIG. 3. Model calculations based on the Drude parameters in Table I. (a) The reflectance spectrum of the Drude model at near-normal incidence. (b) The TDR spectrum of the Drude model with a $\Delta T=5$ K. The structure in the TDR spectrum is a result of the temperature-dependent changes in the material's plasma frequency and optical scattering rate. The location of the screened plasma frequency $\tilde{\omega}_p$ is indicated by the arrow in the figure.

TABLE I. Drude and modified Drude optical parameters. Parameters used to model the reflectance and TDR spectra of a Drude and a modified Drude metal shown in Figs. 3 and 4. The optical properties of a Drude metal are determined by the bare plasma frequency, ω_p, the high-frequency dielectric constant, ϵ_∞, and the optical scattering rate, Γ. The TDR spectrum of a Drude metal is determined by the temperature dependence of both the unit-cell volume and the scattering rate. The modified Drude metal is taken to be one in which the scattering rate is linearly dependent on frequency.

Model	ω_p (eV)	ε_∞	Γ (eV)	$\frac{1}{V}\frac{\partial V}{\partial T}$ (K^{-1})	$\frac{\partial\Gamma}{\partial T}$ (eV K^{-1})
Drude	3.0	4.0	0.3	10^{-5}	k_B
Modified Drude	3.0	4.0	0.6ω	10^{-5}	k_B

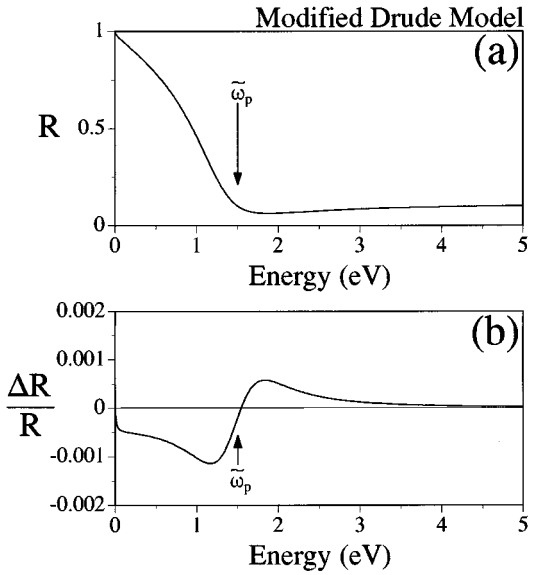

FIG. 4. Model calculations based on the modified Drude parameters in Table I. (a) The reflectance spectrum of the modified Drude model at near-normal incidence. This reflectance spectrum is similar to the reflectance spectra of the cuprate superconductors. (b) The TDR spectrum of the modified Drude model with a $\Delta T=5$ K. The location of the screened plasma frequency, $\tilde{\omega}_p$, is indicated by the arrow in the figure. Unlike the TDR in the Drude model, $\tilde{\omega}_p$ lies close to the zero crossing in the modified Drude model.

It is well known that the optical response of the cuprate superconductors is distinctively non-Drude.[46,50,54,56] However, this response can be approximated phenomenologically by a modified Drude model in which the optical scattering rate is both temperature and energy dependent. Schlesinger *et al.*,[50] proposed that the optical scattering rate in the cuprates could be written as

$$\Gamma = \max(k_B T, A\omega), \tag{10}$$

where A is approximately 0.6, and $\max(\cdots)$ represents that the larger of the two quantities is to be taken. A similar form of optical scattering rate has been derived in the context of a nested Fermi liquid[72] and in marginal Fermi liquid theory.[73–75] Although this form of Γ implies a causal change in the optical effective mass m^*, this change is small at the energies of interest ($\sim$1.0 eV) and we neglect it. This form of scattering rate directly affects the form of the reflectance spectrum. The R of this model, calculated using the modified Drude parameters in Table I, is shown in Fig. 4(a). Instead of possessing an abrupt decrease in R at $\tilde{\omega}_p$, the reflectance is seen to decrease nearly linearly with increasing energy. This energy-dependent behavior of R makes it difficult to determine $\tilde{\omega}_p$ directly from the data. Instead, numerous techniques involving the Kramers-Kronig transformation of R, and optical sum rule arguments,[54] are utilized in an attempt to determine the optical parameters.

The TDR spectrum of this modified Drude model is shown in Fig. 4(b). As in the conventional Drude model, there is a large derivative structure located near $\tilde{\omega}_p$ which allows for the direct determination of $\tilde{\omega}_p$ to within the experimental uncertainties obtained by other methods.[54] As can be seen in Fig. 4(b), $\tilde{\omega}_p$ lies close to the zero crossing in the modified Drude TDR spectrum. This demonstrates a unique feature of TDR spectra of metals. Though the location of the screened plasma frequency is obscured in the conventional reflectance measurement, its location is quite apparent in the TDR spectrum. We find that, in general, as Γ increases, $\tilde{\omega}_p$ tends to be closer to the zero crossing in the TDR spectrum. Similarly, as Γ becomes smaller, $\tilde{\omega}_p$ tends towards the negative peak in the TDR spectrum. Thus, an approximate $\tilde{\omega}_p$ may be obtained directly by measuring the energies of the negative peak and the zero crossing in the TDR spectrum of Drude-like metals.

B. Normal-state thermal-difference reflectance spectra of cuprate superconductors

The normal-state TDR spectra of Tl-2223, Tl-2212, BiPb-2223, and YBCO are shown in Fig. 5. All of these spectra were measured at 300 K and at a temperature just above each sample's T_c between photon energies of 0.3 and 4.5 eV with a $\Delta T=5$ K. The TDR spectra of all these materials are qualitatively similar. For example, they all possess a large derivative structure near 1.0 eV. This structure is known to arise from the temperature-induced changes in both the scattering rate and the volume of the material's unit cell, as discussed previously. From these TDR spectra, we have graphically determined the location of $\tilde{\omega}_p$ for each material. These values are shown in Table II where we take $\tilde{\omega}_p$ to be the average of the energies of the negative peak in the TDR spectrum and the zero crossing. The plasma response of YBCO, Fig. 5(d), is unique in that it is the only orthorhombic material studied, and thus is known to possess two distinct in-plane plasma frequencies. These correspond to the so-called plane and chain contributions to the optical properties of the material.[50,51] The existence of two in-plane plasma frequencies, which is difficult to measure in unpolarized reflectance spectroscopy, is clearly evident in the TDR spectrum of YBCO.

In addition to the plasma response, there is significant structure in the TDR spectra of these materials at photon energies greater than $\tilde{\omega}_p$. In particular, all of the materials possess structure in their TDR spectrum between 3.0 and 4.0 eV. This structure most likely corresponds to the thermal derivative of charge-transfer excitations in these materials. The Tl-2212 spectrum shows a particularly strong effect. This structure arises mainly from the temperature-induced changes in the energy position of this transition, and, by the nature of the transition, is most dramatically affected by the changes in the volume of the unit cell with temperature. In addition, the TDR spectra of both Tl-2212 and YBCO show structure near 1.7 and 2.0 eV, respectively. This structure is most likely the TDR response of a $d^9-d^{10}\underline{L}$ Cu-O charge-transfer excitation which is known to exist in materials possessing Cu-O based planes.[47,76–78] This optical structure may be obscured in the Tl-2223 and BiPb-2223 spectra because of the location of the TDR screened plasma response.

The temperature dependence of the TDR spectra of these materials in the normal state yields information on the temperature dependence of both the coefficient of thermal expansion and the optical scattering rate. The optical scattering rate in the cuprates is most commonly described by Eq. (10). The linear temperature dependence of this scattering rate is consistent with the observed linear temperature-dependent

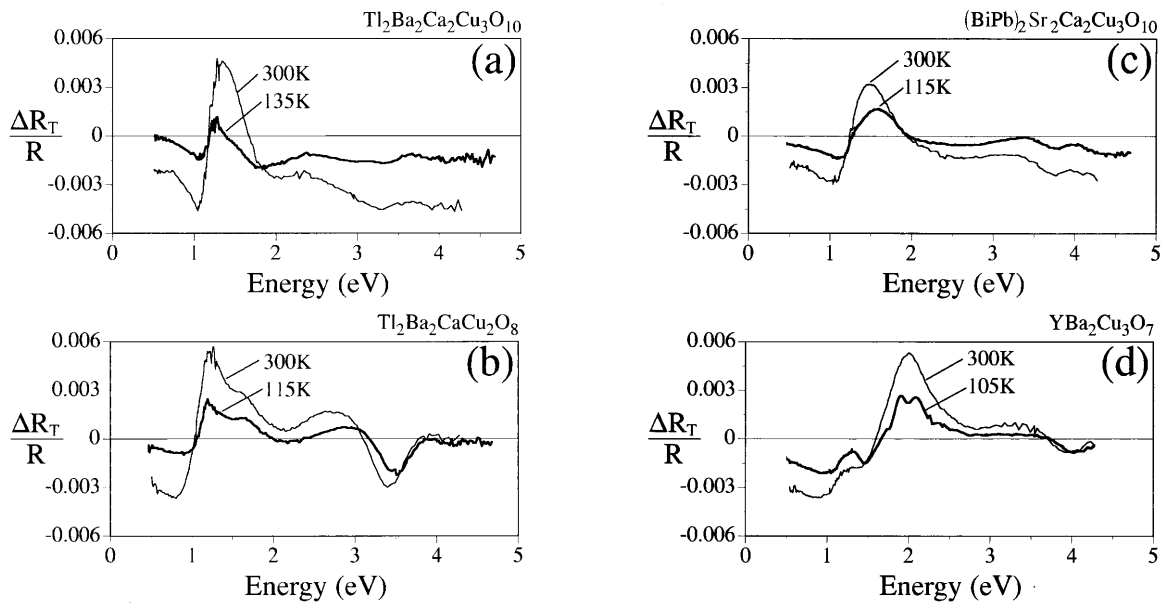

FIG. 5. The normal-state TDR spectra of (a) $Tl_2Ba_2Ca_2Cu_3O_{10}$ ($T_c \sim 118$ K), (b) $Tl_2Ba_2CaCu_2O_8$ ($T_c \sim 105$ K), (c) $(BiPb)_2Sr_2Ca_2Cu_3O_{10}$ ($T_c \sim 106$ K), and (d) $YBa_2Cu_3O_7$ ($T_c \sim 91$ K). For each sample, data are shown at 300 K and at a temperature just above the sample's T_c. The amplitude of the TDR spectrum of each sample is observed to depend linearly on temperature, indicating that the optical scattering rate scales at T^2.

resistivity of these materials, which is essentially a measure of the scattering rate in the limit of zero frequency. Because the optical scattering rate depends linearly on temperature in the modified Drude model and is dominated by the ω-dependent contribution at the energies of interest, the contribution of this term to the temperature dependence of the TDR spectrum is negligible. Consequently, the *temperature dependence* of the TDR spectrum in the modified Drude model is dominated by the temperature-dependent changes in the thermal-expansion coefficient. To illustrate these temperature-dependent effects, we have calculated the TDR spectrum of the modified Drude model shown in Fig. 4(b) at 300 and 100 K. The results of these calculations are shown in Fig. 6 where we use Eq. (10) for the optical scattering rate and the measured temperature-dependent lattice parameters of YBCO for both V and dV/dT.[79] From Fig. 6 it is clearly seen that the TDR spectrum in the modified Drude model is nearly independent of temperature and that, in general, the amplitude of the TDR spectrum at higher temperatures decreases due to the increase in the size of the unit cell.

This temperature-dependent behavior is in stark contrast to that observed in the temperature-dependent TDR spectra of the cuprate superconductors (Fig. 5). We find that the amplitude of the TDR spectra of these materials from 300 to approximately 100 K varies approximately *linearly* with temperature. This behavior is illustrated in Fig. 7 where the amplitude of the positive maximum in the TDR spectrum of Tl-2223 is plotted versus temperature. Because the changes in the lattice with temperature cannot account for this behavior, this result suggests that the temperature dependence of the *optical scattering rate* scales as T^2. We note that a T^2 temperature dependence of the scattering rate *does not agree* with the observed T dependence of the resistivity in the cuprates. This may arise because the resistivity is a measure of the scattering rate near the Fermi surface, or essentially at zero frequency, while the TDR spectrum probes the temperature dependence of the scattering rate at optical frequencies. Thus, from this experimental observation, we propose that the temperature-dependent *optical* scattering rate in these materials is of the form,

$$\Gamma = A(k_B T)^2 + B\omega, \tag{11}$$

where A and B are constants. We have retained a term in the scattering rate that is *linear* with ω because it well describes

TABLE II. Screened plasma frequencies obtained graphically from the TDR spectra. Values of the screened plasma frequencies, $\tilde{\omega}_p \sim (\omega_p/\sqrt{\varepsilon_\infty})$, obtained graphically from the TDR spectra of the cuprate superconductors shown in Fig. 5. We take the magnitude of $\tilde{\omega}_p$ to be the average between the most negative peak in the TDR plasma response and the zero crossing.

Sample	TDR negative peak (eV)	TDR zero crossing (eV)	$\tilde{\omega}_p$ (eV)
T1-2223	1.04	1.17	1.11±0.07
T1-2212	0.79	1.03	0.91±0.12
BiPb-2223	1.04	1.24	1.14±0.10
YBCO	1.37	1.59	1.48±0.11
	0.88	1.18	1.03±0.15

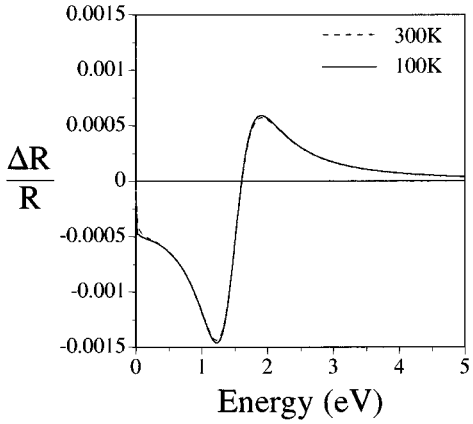

FIG. 6. Calculated TDR spectrum at 300 and 100 K based upon the temperature-dependent lattice parameters of $YBa_2Cu_3O_7$ and an optical scattering rate Γ equal to $\max(k_BT,0.6\omega)$. This model, unlike the TDR response observed in the cuprate superconductors, yields a TDR spectrum which is virtually *independent* of temperature from 300 to 100 K.

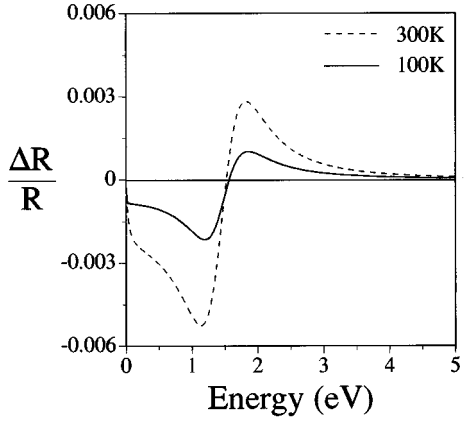

FIG. 8. Calculated TDR spectrum at 300 and 100 K based upon the temperature-dependent lattice parameters of $YBa_2Cu_3O_7$ and an optical scattering rate Γ equal to $B(k_BT)^2+0.6\omega$, with $B=100$ eV^{-1}. This model, like the TDR response observed in the cuprate superconductors, yields a TDR spectrum which is *linearly dependent* on temperature from 300 to 100 K.

the reflectance spectrum of the cuprate superconductors.[80] In Fig. 8 the TDR spectrum of the modified Drude model, using the scattering rate shown in Eq. (11), is plotted at 300 and 100 K. It is easily seen that, similar to the temperature-dependent TDR response of the cuprate superconductors, the amplitude of the TDR signal in this model is linearly dependent on T.

C. Superconducting-state thermal-difference reflectance spectra of cuprate superconductors

The low-temperature TDR spectra of T1-2223, T1-2212, BiPb-2223, and YBCO are shown in Fig. 9. For each sample, the TDR spectrum is shown at temperatures immediately above the sample's T_c, and at temperatures well into the superconducting state. Upon entering the superconducting state, there is a significant *increase* in the amplitude of the structure in the TDR spectrum of each sample. This is in stark contrast to the behavior of the spectra at temperatures above T_c, where the amplitude of the structure in the TDR spectrum of each sample tends to *decrease* with temperature. Since this same effect is observed in all of the different materials, each with a different T_c, we associate this change in the optical properties with the onset of superconductivity. In principle, the change in the TDR spectrum at T_c contains information about the underlying superconducting gap function. To facilitate the interpretation of these spectra, we have developed a normalization procedure from which it is possible to obtain the superconducting to normal-state reflectance ratio directly from the raw TDR spectra.

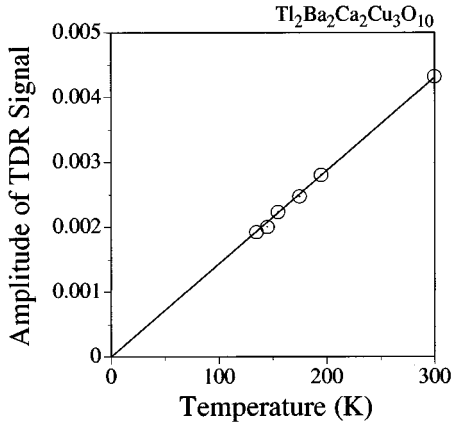

FIG. 7. The amplitude of the positive maximum in the TDR response of $Tl_2Ba_2Ca_2Cu_3O_{10}$ as a function of temperature. The linear dependence of the amplitude of the TDR structure is evident in the figure.

D. Calculation of the superconducting to normal-state reflectance ratio from TDR spectra

Since the TDR spectrum of each sample is proportional to temperature for T1-2223 and YBCO, or virtually independent of temperature for BiPb-2223 and T1-2212, at temperatures just above the material's T_c, it is possible to remove the normal-state TDR response from the TDR data collected below T_c to show more clearly the structure in the spectra which results from the onset of superconductivity. This normalization procedure results in data that are proportional to the superconducting to normal-state reflectance ratio, R_S/R_N, spectrum of the material at temperatures just below the material's T_c. It is analogous to the division of the superconducting state conductance spectra by the normal-state conductance typically performed in $N/I/S$ tunneling measurements.[4]

To illustrate this normalization procedure, we concentrate on the temperature-dependent TDR spectrum of T1-2223. The critical temperature of this material was determined to be approximately 118 K. We take the normal-state TDR spectrum as the data collected at 135 K. Recalling Eq. (2), these data represent the normalized difference in the reflectance of the material collected at 140 and 130 K ($\Delta T=5$ K). Thus, within the temperature range of the measurement, the sample is completely in the normal state. The temperature dependence of the amplitude of the TDR spectrum for T1-2223 is observed to be proportional to temperature at tem-

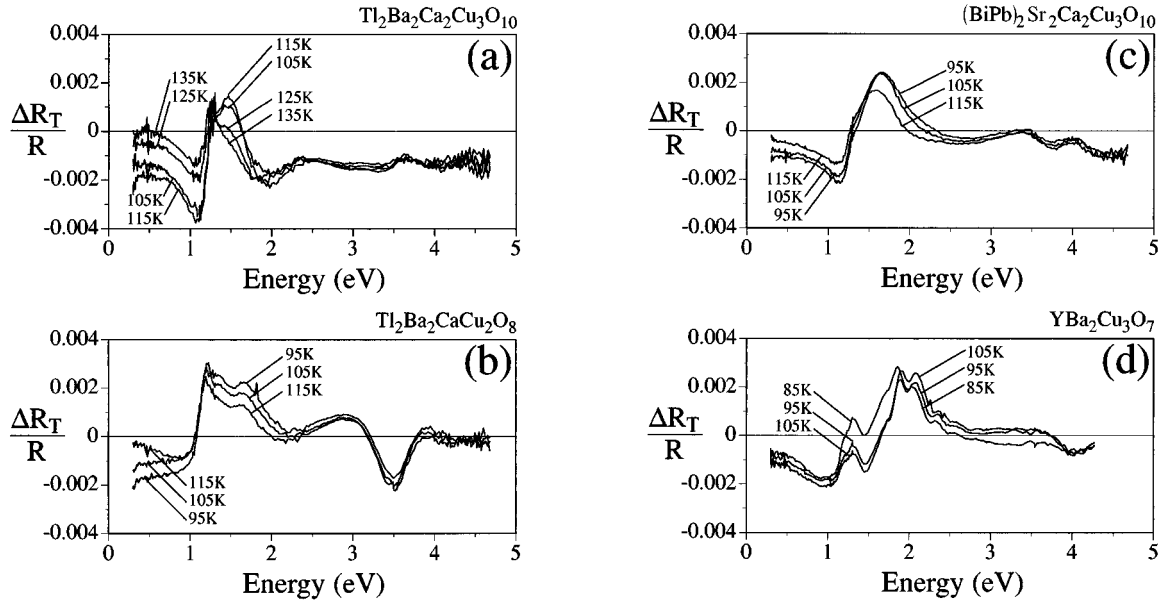

FIG. 9. The TDR spectra of (a) $Tl_2Ba_2Ca_2Cu_3O_{10}$ ($T_c \sim 118$ K). (b) $Tl_2Ba_2CaCu_2O_8$ ($T_c \sim 105$K), (c) $(BiPb)_2Sr_2Ca_2Cu_3O_{10}$ ($T_c \sim 106$ K), and (d) $YBa_2Cu_3O_7$ ($T_c \sim 91$ K) at the indicated temperatures. For each sample, data are shown at temperatures corresponding to both the normal state and the superconducting state of the sample. We observe additional structure between 1.0 and 2.0 eV in the TDR spectra collected at temperatures below each sample's superconducting critical temperature.

peratures above T_c.[60] Thus, we assume the temperature dependence of the material at any temperature *if it were in the normal state* can be expressed as

$$\frac{\Delta R_T^N}{R} = \left(\frac{T}{135\ \mathrm{K}}\right) \frac{\Delta R_{135\ \mathrm{K}}}{R}, \tag{12}$$

where the superscript N indicates that this represents strictly the normal-state response of the material. With Eq. (12) we may extrapolate the normal-state TDR response of the material into the superconducting state. This procedure is justified empirically because if we perform the same procedure for temperatures greater than the normalization temperature (i.e., 135 K for T1-2223) we find that the measured TDR spectra and the extrapolated spectra are virtually identical.

The R_S/R_N of the material can be obtained by subtracting the extrapolated normal-state TDR spectrum from the measured TDR spectrum of the material collected at a temperature which cycles in and out of the superconducting state. For T1-2223, the spectra collected at 115 K cycles between the superconducting and normal state. The subtraction of the extrapolated TDR spectrum from the measured TDR spectrum at 115 K yields

$$\frac{\Delta R_{115\ \mathrm{K}}}{R} - \frac{\Delta R_{115\ \mathrm{K}}^N}{R} = \frac{R_{120\ \mathrm{K}} - R_{110\ \mathrm{K}}}{\langle R \rangle} - \frac{R_{120\ \mathrm{K}}^N - R_{110\ \mathrm{K}}^N}{\langle R \rangle}, \tag{13}$$

which can easily be shown to be

$$\frac{\Delta R_{115\ \mathrm{K}}}{R} - \frac{\Delta R_{115\ \mathrm{K}}^N}{R} = 1 - \frac{R_{110\ \mathrm{K}}^S}{R_{110\ \mathrm{K}}^N}, \tag{14}$$

with the assumption that the normal-state reflectance of the material at 110 K is approximately equal to the average value of the reflectance, $\langle R \rangle$. Thus, the superconducting to normal-state reflectance ratio of T1-2223 at 110 K can be written as

$$\frac{R_S}{R_N} = \frac{R_{110\ \mathrm{K}}^S}{R_{110\ \mathrm{K}}^N} = 1 - \left\{ \frac{\Delta R_{115\ \mathrm{K}}}{R} - \frac{\Delta R_{115\ \mathrm{K}}^N}{R} \right\}. \tag{15}$$

The R_S/R_N of T1-2223 at 110 K obtained in this manner is shown in Fig. 10(a). This R_S/R_N is seen to possess a significant amount of structure at photon energies as high as 2.0 eV. The R_S/R_N of T1-2212, BiPb-2223, and YBCO are shown as (b), (c), and (d) in Fig. 10, respectively. The normalization procedure for both T1-2223 and YBCO follow what is described above. The normalization procedure for T1-2212 and BiPb-2223, however, did not utilize the linear temperature-dependent extrapolation because the TDR spectra of these materials were observed to be virtually independent of temperature for temperatures just above T_c, although this approximate linear-T dependence is observed from 300 to $\sim$120 K in these materials.

In each sample, there is considerable structure in the reflectance ratio at high photon energies. This structure is related to the onset of superconductivity and thus contains information about the energy dependence of the superconducting gap function, $\Delta(\omega)$. In the following sections, we extract information pertaining to the functional form of $\Delta(\omega)$, and the underlying electron-boson coupling function, $G(\omega)$, based upon a generalized Eliashberg description of the superconducting state, and the associated strong-coupling description of the optical properties of a superconductor.

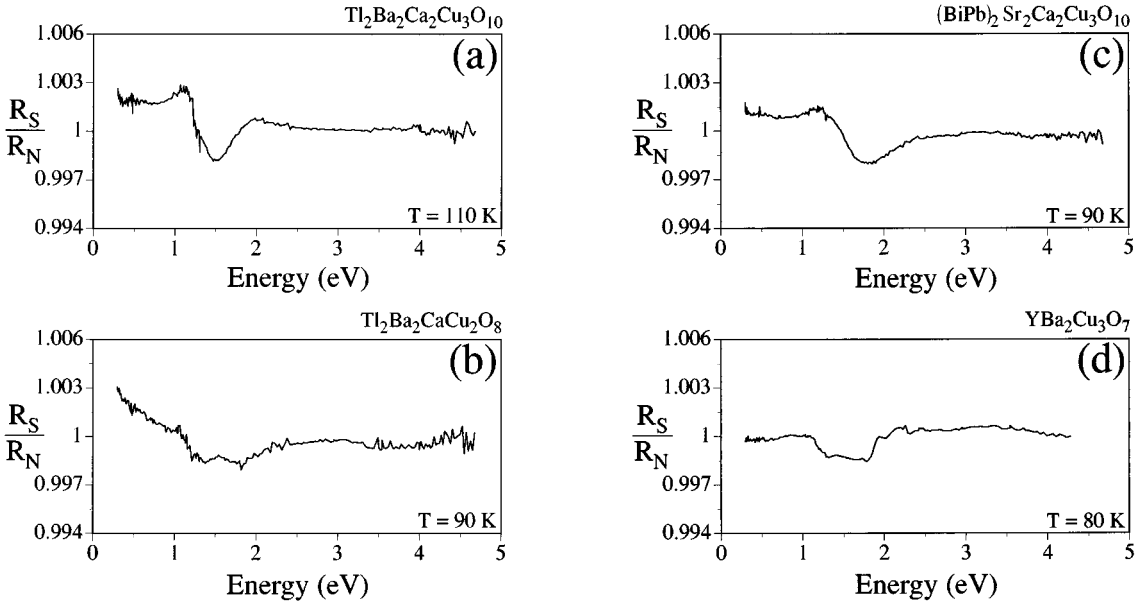

FIG. 10. The superconducting to normal-state reflectance ratio, R_S/R_N, of (a) $Tl_2Ba_2Ca_2Cu_3O_{10}$ at $T=110$ K, (b) $Tl_2Ba_2CaCu_2O_8$ at $T=90$ K, (c) $(BiPb)_2Sr_2Ca_2Cu_3O_{10}$ at $T=90$ K, and (d) $YBa_2Cu_3O_7$ at $T=80$ K. For all samples, R_S/R_N deviates significantly from unity at energies as high as 2.5 eV.

IV. DATA ANALYSIS

We analyze our results based upon the following model assumptions. First, we assume an isotropic Eliashberg model describing both the optical properties and the superconducting gap function. Even though the cuprate superconductors are highly anisotropic, this assumption has some merit in that we have measured the optical properties with unpolarized light in the copper-oxygen plane of the material. In the end, although we cannot measure $G(\omega,\mathbf{k})$ from the unpolarized TDR data, it is possible to obtain information about $G(\omega)$ in these materials. Like $N/I/S$ tunneling measurements, we are essentially taking an average of $G(\omega,\mathbf{k})$ over the Fermi surface. This simplifies dramatically the equations involved in calculating the optical properties of an Eliashberg superconductor.

We also assume that the changes in the optical properties which occur when the material passes into the superconducting state arise from the existence of a finite $\Delta(\omega,T)$ at temperatures below T_c, and neglect the minor changes in the unit cell that are known to occur in the neighborhood of T_c in these materials.[79,81–85] This assumption is justified by the arguments, and theoretical TDR calculations, discussed in Sec. II B. In the end, we find that the changes in the amplitude of the TDR spectrum which may occur with an associated structural change at T_c alter the amplitude of the TDR spectrum only a fraction of a percent of the measured amplitude. Further, a simple discontinuous change in the structure of the unit cell cannot account for the *different spectral form* of the TDR structure which grows in at T_c, as evidenced most clearly in T1-2223 [115 K spectrum in Fig. 9(a)].

A. Formalism

In our model, we assume the Eliashberg theory of superconductivity is an appropriate formalism to describe the superconducting state of these materials. The existence of a complex, energy-dependent gap function will necessarily modify the optical scattering time of the material. The scattering time of the material in the superconducting state, $\tau_S(\omega)$, may be calculated by assuming a form for the scattering time of the material in the normal state, $\tau_N(\omega)$.[34,35] From this, the superconducting to normal-state reflectance ratio may be calculated and compared to experiment.

The procedure we use to calculate a theoretical R_S/R_N is as follows. We first assume a functional form of the electron-boson coupling function, $G(\omega)$, and a magnitude of the Coulomb repulsion, μ^*, to match the experimentally measured T_c. The theoretical T_c is the temperature at which $\Delta(\omega,T)$ equals zero. Thus, we can find T_c for a model $G(\omega)$ and μ^* by solving for $\Delta(\omega,T)$ at a variety of temperatures and finding the temperature at which $\Delta(\omega,T)$ collapses to zero. We obtain $\Delta(\omega,T)$ based upon $G(\omega)$, T, and μ^* using the finite temperature, real-energy axis formulation of the Eliashberg integral equations. In an isotropic model, these equations can be written as[3]

$$\Delta(\omega,T)=\frac{1}{Z(\omega,T)}\int_0^\infty d\omega'\ \mathrm{Re}\left\{\frac{\Delta(\omega',T)}{\sqrt{\omega'^2-\Delta^2(\omega',T)}}\right\}\times K_+(\omega,\omega',T)-\frac{\mu^*}{Z(\omega,T)}\int_0^\infty d\omega'\times\mathrm{Re}\left\{\frac{\Delta(\omega',T)}{\sqrt{\omega'^2-\Delta^2(\omega',T)}}\right\}\tanh\left(\frac{\beta\omega'}{2}\right), \quad (16)$$

with

$$Z(\omega,T)=1-\frac{1}{\omega}\int_0^\infty d\omega'\ \mathrm{Re}\left\{\frac{\omega'}{\sqrt{\omega'^2-\Delta^2(\omega',T)}}\right\}\times K_-(\omega,\omega',T), \quad (17)$$

$$K_+(\omega,\omega',T)=\int_0^\infty d\Omega\ G(\Omega)\left[\frac{f(-\omega')+n(\Omega)}{\omega'+\omega+\Omega}+\frac{f(-\omega')+n(\Omega)}{\omega'-\omega+\Omega}-\frac{f(\omega')+n(\Omega)}{-\omega'+\omega+\Omega}-\frac{f(\omega')+n(\Omega)}{-\omega'-\omega+\Omega}\right], \tag{18}$$

$$K_-(\omega,\omega',T)=\int_0^\infty d\Omega\ G(\Omega)\left[\frac{f(-\omega')+n(\Omega)}{\omega'+\omega+\Omega}-\frac{f(-\omega')+n(\Omega)}{\omega'-\omega+\Omega}+\frac{f(\omega')+n(\Omega)}{-\omega'+\omega+\Omega}-\frac{f(\omega')+n(\Omega)}{-\omega'-\omega+\Omega}\right], \tag{19}$$

and

$$f(\omega)=\left(\frac{1}{\exp(\beta\omega)+1}\right),\quad n(\omega)=\left(\frac{1}{\exp(\beta\omega)-1}\right),$$

where $\Delta(\omega,T)$ is the complex, energy- and temperature-dependent superconducting gap function, $Z(\omega,T)$ is the complex, energy- and temperature-dependent renormalization function, $G(\Omega)$ is the generalized energy-dependent electron-boson coupling function averaged over the Fermi surface, μ^* is the screened Coulomb repulsion, $f(\omega)$ and $n(\omega)$ are the Fermi and Bose occupation factors, respectively, and $\beta=1/k_BT$. Together, these equations form a nonlinear set of coupled integral equations which must be solved self-consistently for $\Delta(\omega,T)$.

A full description of the procedures used to solve the finite temperature real-energy axis Eliashberg equations has been described previously.[86] Briefly, an iterative procedure is used to solve such integral equations. If $G(\omega)$, μ^*, and T are known, then the real and imaginary components of $K_\pm(\omega,\omega',T)$ are calculated and stored for all points $\{\omega,\omega'\}$. Then, using the calculated $K_\pm(\omega,\omega',T)$ and a guess at the initial form of $\Delta(\omega,T)$. Eqs. (16) and (17) are iterated until the solution is self-consistent. Specifically, the first-order guess for $\Delta(\omega,T)$ is usually taken as a constant, real quantity with a magnitude approximately that of a typical BCS gap. With this first-order guess of $\Delta(\omega,T)$, the renormalization function $Z(\omega,T)$ is calculated using Eq. (17). Then a new $\Delta(\omega,T)$ is calculated using Eq. (16), the first-order guess at $\Delta(\omega,T)$, and the newly calculated $Z(\omega,T)$. This iteration procedure is repeated until the newly calculated $\Delta(\omega,T)$ does not differ significantly from the solution of the previous iteration.

With a model $G(\omega)$ and μ^* that matches the observed T_c, and the $\Delta(\omega,T)$ obtained from the solution of the Eliashberg equations at the temperature at which the superconducting to normal-state reflectance ratio is collected, we calculate the reflectance in both the superconducting and normal states according to the following method. With a knowledge of $\Delta(\omega,T)$ it is possible to express the real part of the optical conductivity in the superconducting state, $\mathrm{Re}\{\sigma_S(\omega,T)\}$, in terms of the real part of the optical conductivity in the normal state, $\mathrm{Re}\{\sigma_N(\omega,T)\}$. It can be shown that the ratio of $\mathrm{Re}\{\sigma_S(\omega,T)\}$ to $\mathrm{Re}\{\sigma_N(\omega,T)\}$ at low temperatures can be written as[35]

$$\frac{\mathrm{Re}\{\sigma_S(\omega)\}}{\mathrm{Re}\{\sigma_N(\omega)\}}=\frac{2}{\omega}\int_0^{\omega/2}d\tilde{\omega}\ \mathrm{Re}\left(\frac{\tilde{\omega}}{\sqrt{\tilde{\omega}^2-\Delta^2(\tilde{\omega})}}\right)\times\mathrm{Re}\left(\frac{\omega-\tilde{\omega}}{\sqrt{(\omega-\tilde{\omega})^2-\Delta^2(\omega-\tilde{\omega})}}\right)-\frac{2}{\omega}\int_0^{\omega/2}d\tilde{\omega}\ \mathrm{Re}\left(\frac{\Delta(\tilde{\omega})}{\sqrt{\tilde{\omega}^2-\Delta^2(\tilde{\omega})}}\right)\times\mathrm{Re}\left(\frac{\Delta(\omega-\tilde{\omega})}{\sqrt{(\omega-\tilde{\omega})^2-\Delta^2(\omega-\tilde{\omega})}}\right). \tag{20}$$

Equation (20) is valid in both the extreme anomalous (l and $\xi\gg\lambda$) and London (l and $\xi\ll\lambda$) limits, where l is the electron mean free path, ξ is the superconducting coherence length, and λ is the optical penetration depth. At the photon energies of interest, the cuprate superconductors are taken to be in the London limit. If we assume a model for $\sigma_N(\omega,T)$, it is possible to calculate $\sigma_S(\omega,T)$ using $\Delta(\omega,T)$ and Eq. (20). In our model, we assume a modified Drude description of the normal-state optical properties of the materials and use a normal-state scattering rate, $\Gamma(\omega,T)=1/\tau_N(\omega,T)$, of the form in Eq. (11). The complex optical conductivity in the Drude model can be written as[87]

$$\sigma(\omega,T)=\frac{\sigma_{\mathrm{dc}}}{1-i\omega\tau}, \tag{21}$$

where σ_{dc} is the zero-frequency conductivity of the material, and τ is the scattering time, which we take to be both frequency and temperature dependent. Using Eqs. (20) and (21) it can be shown that the scattering time in the superconducting state $\tau_S(\omega,T)$ can be expressed as,

$$\tau_s(\omega,T)=\frac{1+\omega^2\tau_N^2(\omega,T)}{2\omega^2\tau_N(\omega,T)\,\theta(\omega,T)}+\frac{\sqrt{\omega^2\tau_N^2(\omega,T)-2\omega\tau_N(\omega,T)\,\theta(\omega,T)+1}\,\sqrt{\omega^2\tau_N^2(\omega,T)+2\omega\tau_N(\omega,T)\,\theta(\omega,T)+1}}{2\omega^2\tau_N(\omega,T)\,\theta(\omega,T)}, \tag{22}$$

TABLE III. Example model systems used in an attempt to fit the experimental R_S/R_N spectra. The parameters used to model the experimental R_S/R_N data. The electron-boson coupling function used as input to the Eliashberg equations consists of both an electron-phonon and, in the midinfrared and near-infrared models, a higher energy electron-boson component. These components are cutoff Lorentzian peaks with amplitudes (A_0,A_1), energies (ω_0,ω_1), and widths (Γ_0,Γ_1) shown. Using the indicated value of the screened Coulomb repulsion, μ^*, the model critical temperature is calculated using the approximate analytic expression for T_C derived by Allen and Dynes. The strength of $G(\omega)$ is varied such that the calculated T_C equals the experimental T_C of each sample. The model R_S/R_N is calculated by using $\Delta(\omega,T)$ obtained by solving the zero-temperature Eliashberg equations and multiplying this solution by the known temperature dependence of a BCS gap. We use the model parameters obtained for $Tl_2Ba_2Ca_2Cu_3O_{10}$ (Table IV) to calculate the R_S/R_N.

Model	A_0	ω_0 (eV)	Γ_0 (meV)	A_1	ω_1 (eV)	Γ_1 (meV)	μ^* (eV)	λ	T_C [a] (K)	Δ_0 (meV)	ω_p (eV)	ε_∞	$1/\tau_N$ (eV)
Phonon	2.0	0.10	15.5				0.10	1.455	118.1	28.02	2.76	4.29	$0.03+0.41\omega$
Phonon+midInfrared	1.9	0.05	7.0	0.795	0.5	100.0	0.15	1.733	118.4	32.80	2.76	4.29	$0.03+0.41\omega$
Phonon+nearInfrared	1.9	0.05	7.0	1.15	1.0	100.0	0.15	1.526	118.1	28.04	2.76	4.29	$0.03+0.41\omega$

[a]Calculated using the approximate analytic expression for T_C derived by Allen and Dynes.

with

$$\theta(\omega,T)=\frac{2}{\omega}\int_0^{\omega/2}d\tilde{\omega}\ \mathrm{Re}\left(\frac{\tilde{\omega}}{\sqrt{\tilde{\omega}^2-\Delta^2(\tilde{\omega},T)}}\right)\times\mathrm{Re}\left(\frac{\omega-\tilde{\omega}}{\sqrt{(\omega-\tilde{\omega})^2-\Delta^2(\omega-\tilde{\omega},T)}}\right)-\frac{2}{\omega}\int_0^{\omega/2}d\tilde{\omega}\times\mathrm{Re}\left(\frac{\Delta(\tilde{\omega},T)}{\sqrt{\tilde{\omega}^2-\Delta^2(\tilde{\omega},T)}}\right)\times\mathrm{Re}\left(\frac{\Delta(\omega-\tilde{\omega},T)}{\sqrt{(\omega-\tilde{\omega})^2-\Delta^2(\omega-\tilde{\omega},T)}}\right). \quad (23)$$

With both $\tau_S(\omega,T)$ and $\tau_N(\omega,T)$, we calculate a model R_S/R_N, vary the optical parameters, ω_p, ϵ_∞, and Γ, within the limits permitted by the 20% uncertainty of the literature values,[54] and attempt to obtain a match with the data. Both the superconducting and normal-state reflectance spectra are calculated for s- and p-polarized light at a 45° angle of incidence. The calculated reflectance ratio is sensitive to the spectral form of $G(\omega)$ used as input to the Eliashberg equations which yield $\Delta(\omega,T)$. If a given $G(\omega)$ does not lead to a satisfactory fit of the measured data with reasonable optical parameters, the shape of $G(\omega)$ is altered, and the entire process is repeated.

We note that in order to calculate R_S/R_N with sufficient accuracy to use the model as a means of fitting our experimental data, it is necessary to both solve for a self-consistent $\Delta(\omega,T)$ and changes in $\tau(\omega,T)$ at the one part in 10^5 level. If this precision is not attained in the numerical calculations of the optical properties of the superconductor, it is not possible to describes changes in the superconducting to normal-state reflectance ratio at the 0.01% level.

B. Comparison of theory and experiment

Having established the numerical procedures required to interpret high precision R_S/R_N data, we first present the results of calculations based upon an interaction that is strictly electron-phonon based. We plot, along with these results, the measured R_S/R_N of the Tl-2223 sample at 110 K for comparison [Fig. 10(a)]. If the superconductivity in Tl-2223 is mediated strictly by either phonons, or any other pairing interaction whose associated electron-boson coupling function is restricted to energies of less than ~100 meV, the optical properties of the material in the superconducting state will reflect this energy dependence. As an example, we choose a cutoff Lorentzian peak model interaction[9] centered at 100 meV with a damping of 15.5 meV. Using a typical μ^* value of 0.1 eV, the amplitude of $G(\omega)$ was raised to a level at which the critical temperature is about 118 K, as obtained from the approximate analytic expression derived by Allen and Dynes for T_C.[19] The model parameters are shown in Table III. These parameters are used as input to the Eliashberg equations to obtain $\Delta(\omega,T)$ at zero temperature. The finite temperature $\Delta(\omega,T)$ is then approximated by multiplying the zero-temperature solution by the known temperature dependence of the BCS gap.[3] Then, using Eq. (22) and (23), and approximate optical parameters for Tl-2223,[88] we calculate the theoretical superconducting to normal-state reflectance ratio.

In Fig. 11, we show the results of these calculations based upon this low-energy coupling function. Figure 11(a) shows the approximate $\Delta(\omega,T)$ at 110 K. It is seen in that there is considerable structure in $\Delta(\omega)$ at low energies, but at energies above approximately 0.6 eV, $\Delta(\omega)$ is very near zero. The R_S/R_N of this model, along with the measured R_S/R_N of Tl-2223, are shown in Fig. 11(b). Clearly, this model represents a poor match to the measured data. The calculated R_S/R_N shows a great deal of structure at energies where there is a finite, large $\Delta(\omega)$. And, as anticipated, very little structure at high energies where the associated structure in the gap function tends to zero.

Even though the calculated R_S/R_N of this model does not fit these data, this result is important because it indicates that, within Eliashberg theory, if the pairing interaction is at energies below approximately 100 meV, like the electron-phonon interaction, then, *no matter how strong the coupling*, the optical properties of the material remain unchanged at energies on the order of 2.0 eV. Since we have observed such changes at these high energies in all of these samples, we conclude that the electron-phonon interaction cannot solely account for the superconductivity in the materials studied in this work.

To illustrate the sensitivity of the calculated R_S/R_N to the form of the input $G(\omega)$, we have calculated the theoretical R_S/R_N based upon a variety of functional forms of the cou-

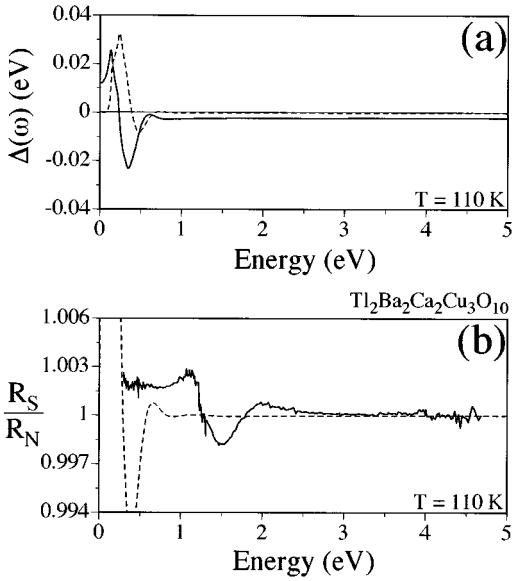

FIG. 11. Calculation of R_S/R_N based upon an electron-boson coupling function which consists only of an electron-phonon interaction. The model parameters are shown in Table III. (a) The real (solid line) and imaginary (dashed line) components of $\Delta(\omega)$ at 110 K. (b) The calculated R_S/R_N (dashed line) shown with the measured R_S/R_N (solid line) of $Tl_2Ba_2Ca_2Cu_3O_{10}$ at 110 K. From the figure it is easily seen that there only is significant structure in the calculated R_S/R_N at energies where there is structure in $\Delta(\omega)$, and that this model interaction does not match the experimental spectrum.

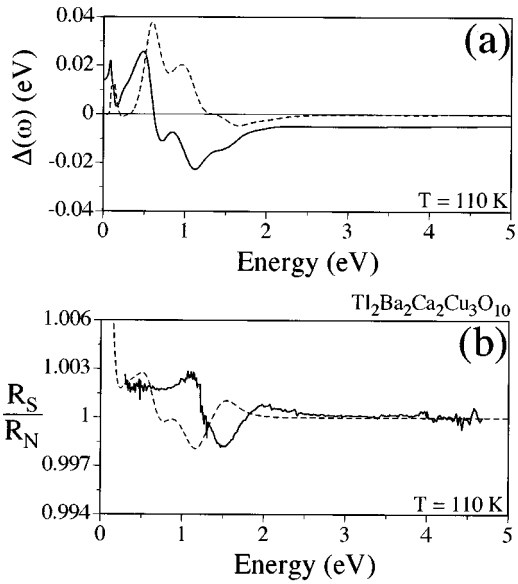

FIG. 12. Calculation of R_S/R_N based upon an electron-boson coupling function which consists of an electron-phonon interaction and a ''midinfrared'' interaction at 0.5 eV. The model parameters are shown in Table III. (a) The real (solid line) and imaginary (dashed line) components of $\Delta(\omega)$ at 110 K. (b) The calculated R_S/R_N (dashed line) shown with the measured R_S/R_N (solid line) of $Tl_2Ba_2Ca_2Cu_3O_{10}$ at 110 K. From the figure it is easily seen that, although there is additional structure in R_S/R_N at higher energies, this model interaction does not match the experimental spectrum.

pling function. These forms include both a low-energy, presumably electron-phonon, and a higher-energy electron-boson interaction. The low-energy electron-boson interaction in all of these calculations is located at 50.0 meV with a broadening of 7.0 meV. The complete model parameters are shown in Table III. Figures 12 and 13 show the $\Delta(\omega,T=110$ K), and R_S/R_N, based upon model interactions which consist of an electron-phonon component *plus* an interaction centered at 0.5 and 1.0 eV, respectively. In each model, there is considerable structure in the reflectance ratio at energies where $\Delta(\omega)$ possesses significant structure, but the calculated R_S/R_N does not match the experimental spectrum.

The best fit of the Tl-2223 R_S/R_N is obtained by including, in addition to the electron-phonon interaction, a high-energy interaction located at 1.6 eV. The model parameters of this fit are shown in Table IV. In this fitting process we have matched the theoretical T_C, calculated by solving the Eliashberg equations at finite temperatures, to the experimental T_C. Figure 14(a), shows the $\Delta(\omega,T)$ obtained by solving the finite-temperature Eliashberg equations at 110 K, and *not* the approximate $\Delta(\omega,T)$ calculated by multiplying the zero-temperature solution by the temperature dependence of the BCS gap. The calculated R_S/R_N based upon this $G(\omega)$ is shown in Fig. 14(b) along with the measured R_S/R_N of Tl-2223. We find very good agreement between the measured and calculated results based upon this coupling model. The zero-temperature solution of the Eliashberg equations based upon this model is shown in Fig. 15, where it is clearly seen that there is considerable structure in both $\Delta(\omega)$ and $Z(\omega)$ at high energies.

Using the same fitting procedure, we show our best fits to date of the Tl-2212 and BiPb-2223 superconducting to

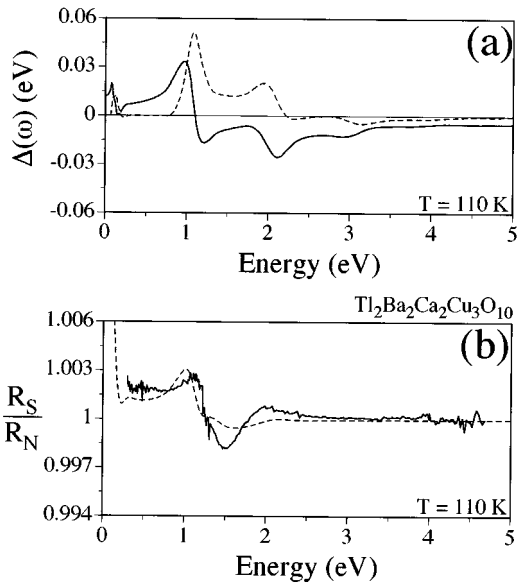

FIG. 13. Calculation of R_S/R_N based upon an electron-boson coupling function which consists of an electron-phonon interaction and a ''near-infrared'' interaction at 1.0 eV. The model parameters are shown in Table III. (a) The real (solid line) and imaginary (dashed line) components of $\Delta(\omega)$ at 110 K. (b) The calculated R_S/R_N (dashed line) shown with the measured R_S/R_N (solid line) of $Tl_2Ba_2Ca_2Cu_3O_{10}$ at 110 K. From the figure it is easily seen that, although there is additional structure in R_S/R_N at higher energies, this model interaction does not match the experimental spectrum.

TABLE IV. Parameters used to fit the experimental R_S/R_N spectra. The parameters used to fit the experimental R_S/R_N data shown in Figs. 15, 16, and 17. The electron-boson coupling function used as input to the Eliashberg equations consists of both an electron-phonon and a high-energy electron-boson component. These components are cutoff Lorentzian peaks with amplitudes ($A_{\rm Ph}$,A_X), energies ($\omega_{\rm Ph}$,ω_X), and widths ($\Gamma_{\rm Ph}$,Γ_X) shown. Using the indicated value of the screened Coulomb repulsion, μ^*, the model critical temperature is calculated to match the experimental T_C of each sample. The experimental R_S/R_N is fit by using $\Delta(\omega,T)$ obtained by solving the finite-temperature Eliashberg equations at the temperature at which the R_S/R_N data are measured, and by varying the magnitude of the bare plasma frequency, ω_p, the high-frequency dielectric constant, ε_∞, and the Drude-like normal-state scattering rate, $1/\tau_N$, within the 20% uncertainty of the literature values.

Sample	T_c [a] (K)	$A_{\rm Ph}$	$\omega_{\rm Ph}$ (eV)	$\Gamma_{\rm Ph}$ (eV)	A_X	ω_X (eV)	Γ_X (eV)	μ^* (eV)	λ	T_C [b] (K)	Δ_0 (meV)	ω_P (eV)	ε_∞	$1/\tau_N$ (eV)
T1-2223	118±1	1.9	0.05	0.007	0.84	1.6	0.20	0.15	1.49	118±0.5	24.41	2.65	4.38	$0.03+0.43\omega$
BiPb-2223	106±1	1.9	0.05	0.007	1.05	2.1	0.18	0.15	1.43	106±0.5	21.55	2.88	4.00	$0.04+0.43\omega$
T1-2212	105±1	1.8	0.05	0.007	1.21	2.0	0.15	0.15	1.37	105±0.5	21.70	2.25	4.05	$0.01+0.51\omega$

[a]Measured using the conventional four-point probe technique.
[b]Calculated using the full finite-temperature Eliashberg equations.

normal-state reflectance ratios. The parameters used in these fits are shown in Table IV. The calculated $\Delta(\omega,T)$ and R_S/R_N of Tl-2212 and BiPb-2223 are shown in Figs. 16 and 17, respectively. While excellent agreement is obtained with the BiPb-2223 data, the Tl-2212 data has a less satisfactory fit. This is not unexpected because of the crudeness of the model used (i.e., the neglect of anisotropy and the modified Drude description of the normal-state optical properties). While it is remarkable that theory and experiment match so well in the Tl-2223 and BiPb-2223 samples, the poorer fit of the Tl-2212 R_S/R_N, particularly in the low-energy region, should not be surprising given the simplicity of the theoretical model. This disagreement could result, for example, from inadequacies in our normalization procedure, an unusual normal-state scattering rate not well described by our model, or our neglect of the causal change in the optical effective

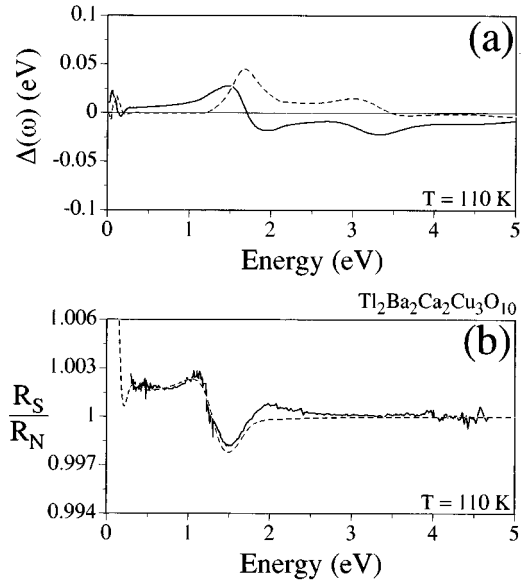

FIG. 14. Calculation of R_S/R_N based upon an electron-boson coupling function which consists of an electron-phonon interaction and an electronic interaction at 1.6 eV. The model parameters are shown in Table IV. (a) The real (solid line) and imaginary (dashed line) components of $\Delta(\omega)$ at 110 K. (b) The calculated R_S/R_N (dashed line) shown with the measured R_S/R_N (solid line) of $Tl_2Ba_2Ca_2Cu_3O_{10}$ at 110 K. From the figure it is easily seen that there is very good agreement between experiment and theory based upon this model interaction.

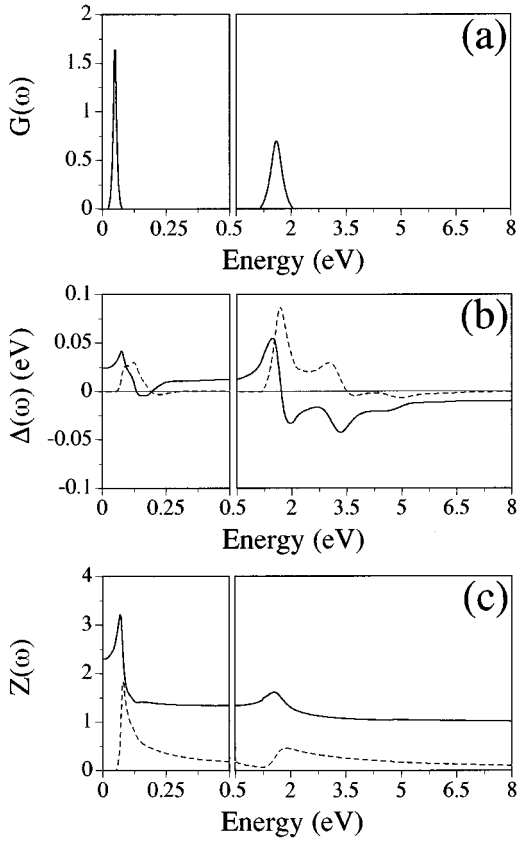

FIG. 15. The Eliashberg model which results in the best fit of the $Tl_2Ba_2Ca_2Cu_3O_{10}$ R_S/R_N data at 110 K. The model parameters are shown in Table IV. (a) A generalized electron-boson coupling function $G(\omega)$ consisting of an electron-phonon interaction at 50 meV and an electronic interaction centered at 1.6 eV. Using this coupling function and the isotropic Eliashberg integral equations, the complex, energy-dependent gap function, $\Delta(\omega)$, and the mass renormalization function, $Z(\omega)$, are calculated. The real (solid line) and imaginary (dashed line) components of both $\Delta(\omega)$ and $Z(\omega)$ are shown in (b) and (c), respectively. Note the change in the energy scale at ω=0.5 eV.

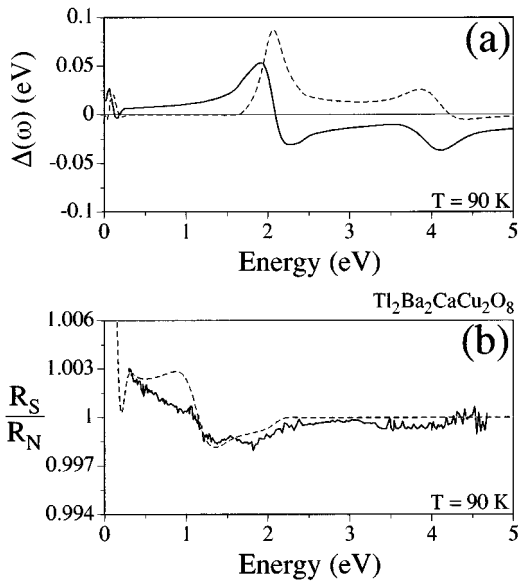

FIG. 16. Calculation of R_S/R_N based upon an electron-boson coupling function which consists of an electron-phonon interaction and an electronic interaction at 2.0 eV. The model parameters are shown in Table IV. (a) The real (solid line) and imaginary (dashed line) components of $\Delta(\omega)$ at 90 K. (b) The calculated R_S/R_N (dashed line) shown with the measured R_S/R_N (solid line) of $Tl_2Ba_2CaCu_2O_8$ at 90 K. From the figure it is seen that, although the match is not as impressive as the R_S/R_N of $Tl_2Ba_2Ca_2Cu_3O_{10}$, there is reasonable agreement between experiment and theory based upon this model interaction.

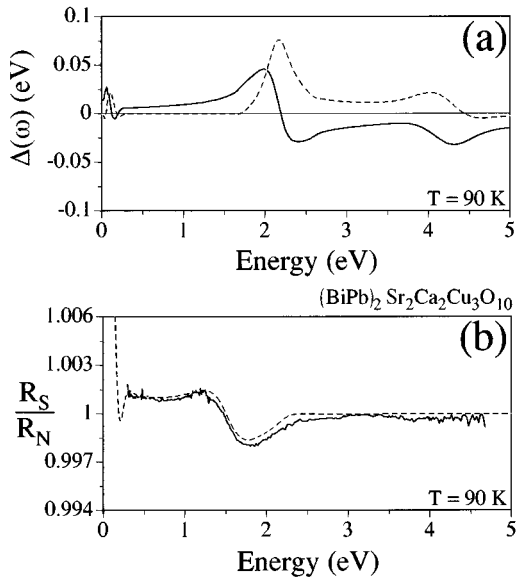

FIG. 17. Calculation of R_S/R_N based upon an electron-boson coupling function which consists of an electron-phonon interaction and an electronic interaction at 2.1 eV. The model parameters are shown in Table IV. (a) The real (solid line) and imaginary (dashed line) components of $\Delta(\omega)$ at 90 K. (b) The calculated R_S/R_N (dashed line) shown with the measured R_S/R_N (solid line) of $(BiPb)_2Sr_2Ca_2Cu_3O_{10}$ at 90 K. From the figure it is seen that there is very good agreement between experiment and theory based upon this model interaction.

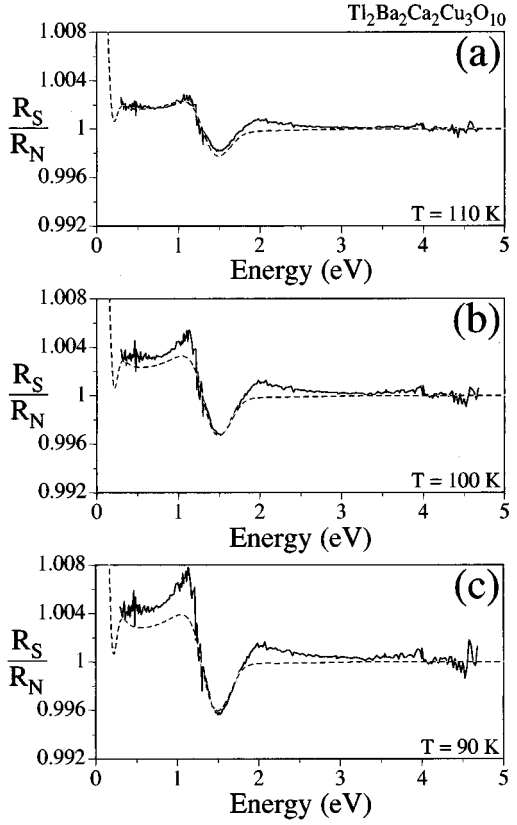

FIG. 18. The experimental (solid line) and calculated (dashed line) superconducting to normal-state reflectance ratio, R_S/R_N, of $Tl_2Ba_2Ca_2Cu_3O_{10}$ at (a) $T=110$ K, (b) $T=100$ K, and (c) $T=90$ K. The spectra are obtained by using the model parameters of Table IV and the calculated temperature dependence of $\Delta(\omega,T)$ at the indicated temperatures.

mass, m^*, which may not be negligible at the lower photon energies. In addition, we have not yet been able to obtain a satisfactory fit of the YBCO R_S/R_N [Fig. 10(d)]. This is presumably because of the complications due to the existence of the two plasma frequencies in the material.[50,51]

The temperature-dependent R_S/R_N spectra of these materials may be obtained from the raw TDR spectra by integrating the normalized TDR response of each sample over temperature for T less than T_C. This procedure is a simple extension of the normalization procedure described previously (Sec. III D) to successively lower temperatures below T_C. The temperature dependence of the R_S/R_N based upon the model parameters shown in Table IV is easily calculated by solving for $\Delta(\omega,T)$ at temperatures below the sample's T_C, and using the normal-state optical parameters obtained from the initial fits (Figs. 15–17). In Figs. 18, 19, and 20 we plot the temperature dependence of the experimental and calculated R_S/R_N of Tl-2223, Tl-2212, and BiPb-2223, respectively.[89] In Tl-2223 and BiPb-2223, there is good agreement between the experimental and theoretical spectra based solely upon the temperature-dependent change in $\Delta(\omega,T)$ which arises naturally from Eliashberg theory. The Tl-2212 spectra, as before, does not agree well with this model description, particularly at low energies.

In making these theoretical fits of the R_S/R_N spectra, no effort was made to improve the agreement by invoking

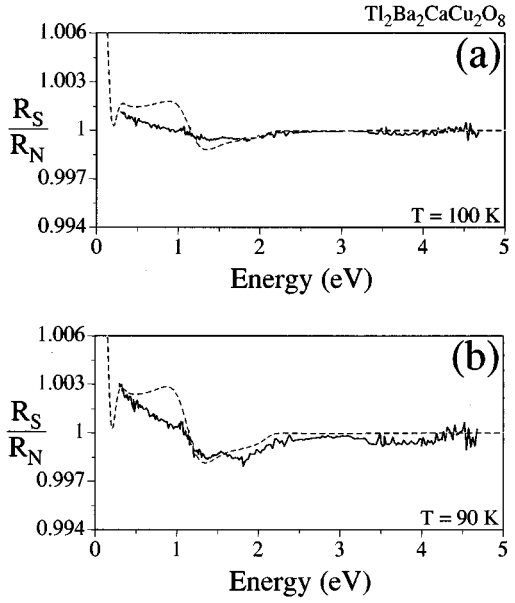

FIG. 19. The experimental (solid line) and calculated (dashed line) superconducting to normal-state reflectance ratio, R_S/R_N, of $Tl_2Ba_2CaCu_2O_8$ at (a) $T=100$ K, (b) $T=90$ K. The spectra are obtained by using the model parameters of Table IV and the calculated temperature dependence of $\Delta(\omega,T)$ at the indicated temperatures.

changes in the normal-state density of states, the effects of anisotropy, the breakdown of particle-hole symmetry or more complex structure in the electron-boson coupling function, all of which could produce a better fit but would have increased the number of adjustable parameters.

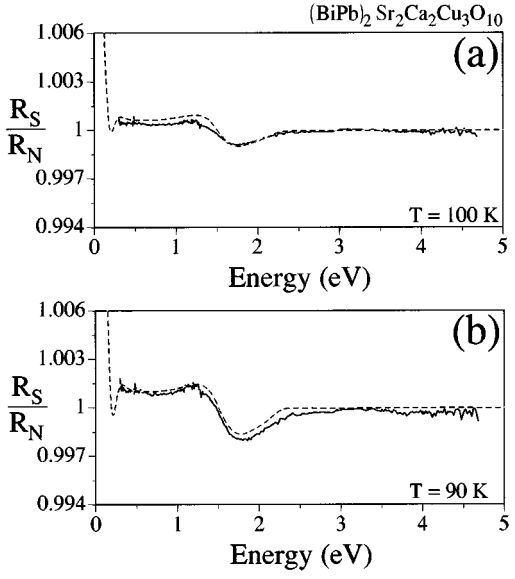

FIG. 20. The experimental (solid line) and calculated (dashed line) superconducting to normal-state reflectance ratio, R_S/R_N, of $(BiPb)_2Sr_2Ca_2Ca_2Cu_3O_{10}$ at (a) $T=100$ K, (b) $T=90$ K. The spectra are obtained by using the model parameters of Table IV and the calculated temperature dependence of $\Delta(\omega,T)$ at the indicated temperatures.

V. CONCLUSIONS

We have shown that the technique of thermal-difference reflectance spectroscopy can provide unique information on temperature-dependent phenomena in the cuprate superconductors. In the normal state of these materials, the temperature-dependent TDR spectra clearly indicate that the optical scattering rate scales as T^2. This is in contrast to the predictions of both nested Fermi liquid theory[72] and marginal Fermi liquid theory,[73–75] and the well-known linear-T dependence of the transport properties of these materials, none of which actually predicts the temperature dependence of the scattering rate at *optical* frequencies. The TDR response of these materials, based upon a Drude-like model, however, is a direct measurement of the temperature dependence of the optical scattering rate. We find that the form of Γ described by Eq. (11) is necessary to account for these experimental results and suggest that an accurate description of the scattering rate in these materials should describe both the T dependence of the scattering rate at zero frequency, and the $(T^2+\omega)$ dependence of the scattering rate at optical frequencies.

The common, and most important feature in the R_S/R_N spectra of Tl-2223, BiPb -2223, Tl-2212, and YBCO is that there is significant deviation from unity at very high photon energies ($\sim$2.0 eV). In order to account for this deviation within Eliashberg theory, the electron-boson coupling function $G(\omega)$ must contain a high-energy component in addition to the known electron-phonon interaction. Only with the existence of this high-energy component of the pairing interaction can we account for the change in the optical properties of these materials at T_C at photon energies of the order of 2.0 eV. Further, because the measured R_S/R_N of these materials cannot be accounted for with a $G(\omega)$ which is only nonzero at low energies ($\sim$100 meV), these results rule out mechanisms of high-temperature superconductivity which involve pairing interactions which are restricted to these low energies. Specifically, these TDR data indicate that an electron-phonon based interaction cannot be solely responsible for the superconductivity in these materials.

Because of the proximity of known charge-transfer excitations[47,76–78] to the energies of the excitations which we require to fit our experimental data for Tl-2223, we had argued that the microscopic origin of this high-energy electron-boson interaction is most likely a d^9-$d^{10}\underline{L}$ Cu-O charge transfer.[60] The present data provide further support for that conjecture and suggest that the charge-transfer excitation contribution to the pairing interaction is a universal feature of the high-temperature ($T_C>40$ K) cuprate superconductors. We have now shown that this effect occurs in both two (Tl-2212) and three-layer (Tl-2223 and BiPb-2223) Cu-O_2 superconductors and is not tied to the presence of thallium, nor to the existence of planes and chains in the crystal structure (YBCO). We predict that all cuprate superconductors with critical temperatures greater than approximately 40 K will show an analogous optical signature at these high energies.

ACKNOWLEDGMENTS

We are indebted to Dr. Wen Y. Lee of IBM Almaden Research Center, San Jose for providing thin films of $Tl_2Ba_2Ca_2Cu_3O_{10}$, Andy Manzi of the University of Califor-

nia, San Diego for thin films of $(BiPb)_2Ba_2Ca_2Cu_3O_{10}$, and Julia M. Phillips of AT&T Bell Laboratories, Murray Hill for thin films of $YBa_2Cu_3O_7$. We thank Gideon Friedmann and Kevin Collins for valuable discussions, comments and criticisms. We acknowledge financial support from the Department of Energy (Grant No. DEFG03-86ER45245-A012). One of us (C.L.P.) acknowledges financial support from the National Science Foundation.

[1] G. M. Eliashberg, Sov. Phys. JETP **11**, 696 (1960).
[2] J. Bardeen, L. N. Cooper, and J. R. Schrieffer, Phys. Rev. **108**, 1175 (1957).
[3] D. J. Scalapino, in *Superconductivity*, edited by R. D. Parks (Dekker, New York, 1969), Vol. 1, p. 449.
[4] W. L. McMillan and J. M. Rowell, in *Superconductivity* (Ref. 3), p. 561.
[5] R. Akis and J. P. Carbotte, Solid State Commun. **78**, 393 (1991).
[6] P. Vashishta and J. P. Carbotte, Phys. Rev. B **7**, 1874 (1972).
[7] J. Blezius *et al.*, Phys. Rev. B **38**, 179 (1988).
[8] R. Akis and J. P. Carbotte, Physica C **157**, 395 (1989).
[9] D. J. Scalapino, J. R. Schrieffer, and J. W. Wilkins, Phys. Rev. **148**, 263 (1966).
[10] A. A. Galkin *et al.*, Sov. Phys. JETP **39**, 1115 (1974).
[11] D. Shimada *et al.*, Z. Phys. B **85**, 7 (1991).
[12] N. Miyakawa *et al.*, J. Phys. Soc. Jpn. **62**, 2445 (1993).
[13] M. Ohuchi *et al.*, Jpn. J. Appl. Phys. **32**, L251 (1993).
[14] M. Ohuchi *et al.*, Jpn. J. Appl. Phys. **32**, L825 (1993).
[15] J. J. Rhyne *et al.*, Phys. Rev. B **36**, 2294 (1987).
[16] B. Renker *et al.*, Z. Phys. B **71**, 437 (1988).
[17] B. Renker *et al.*, Z. Phys. B **77**, 65 (1989).
[18] S. L. Chaplot *et al.*, Physica B **174**, 378 (1991).
[19] J. P. Carbotte, Rev. Mod. Phys. **62**, 1027 (1990).
[20] J. R. Schrieffer, *Theory of Superconductivity* (Benjamin, New York, 1964).
[21] Z. X. Shen *et al.*, Phys. Rev. Lett. **70**, 1553 (1993).
[22] R. K. Kelly *et al.*, Phys. Rev. B **50**, 590 (1994).
[23] H. Ding *et al.*, Phys. Rev. Lett. **74**, 2784 (1995).
[24] T. Staufer *et al.*, Phys. Rev. Lett. **68**, 1069 (1992).
[25] R. Nemetschek *et al.*, Phys. Rev. B **47**, 3450 (1993).
[26] D. Reznik *et al.*, Phys. Rev. B **48**, 7624 (1993).
[27] T. P. Devereaux *et al.*, Phys. Rev. Lett. **72**, 396 (1994).
[28] S. Donovan *et al.*, J. Supercond. **8**, 417 (1995).
[29] T. P. Devereaux, J. Supercond. **8**, 421 (1995).
[30] J. C. Irwin *et al.*, J. Supercond. **8**, 495 (1995).
[31] T. P. Devereaux and D. Einzel, Phys. Rev. B **51**, 16336 (1995).
[32] M. C. Krantz and M. Cardona, Phys. Rev. Lett. **72**, 3290 (1994).
[33] T. P. Devereaux *et al.*, Phys. Rev. Lett. **72**, 3291 (1994).
[34] S. B. Nam, Phys. Rev. **156**, 470 (1967); **156**, 487 (1967).
[35] W. Shaw and J. C. Swihart, Phys. Rev. Lett. **20**, 1000 (1968).
[36] R. E. Glover and M. Tinkham, Phys. Rev. **108**, 243 (1957).
[37] L. H. Palmer and M. Tinkham, Phys. Rev. **165**, 588 (1968).
[38] R. E. Harris and D. M. Ginsberg, Phys. Rev. **188**, 737 (1969).
[39] R. R. Joyce and P. R. Richards, Phys. Rev. Lett. **24**, 1007 (1970).
[40] B. Farnworth and T. Timusk, Phys. Rev. B **10**, 2799 (1974).
[41] B. Farnworth and T. Timusk, Phys. Rev. B **14**, 5119 (1976).
[42] D. Karecki, R. E. Peña, and S. Perkowitz, Phys. Rev. B **25**, 1565 (1982).
[43] Z. Schlesinger *et al.*, Phys. Rev. Lett. **59**, 1958 (1987).
[44] J. Orenstein *et al.*, Physica C **153**, 1740 (1988).
[45] M. Garriga *et al.*, Solid State Commun. **66**, 1231 (1988).
[46] R. T. Collins *et al.*, Phys. Rev. B **39**, 6571 (1989).
[47] M. K. Kelly *et al.*, Phys. Rev. B **40**, 6797 (1989).
[48] J. Humlicek *et al.*, Solid State Commun. **73**, 127 (1990).
[49] Z. Schlesinger *et al.*, Nature (London) **343**, 242 (1990).
[50] Z. Schlesinger *et al.*, Phys. Rev. Lett. **65**, 801 (1990).
[51] A. Zibold *et al.*, Physica C **171**, 151 (1990).
[52] K. Hirochi *et al.*, Jpn. J. Appl. Phys. **29**, L1104 (1990).
[53] H. Romberg *et al.*, Z. Phys. B **78**, 367 (1990).
[54] I. Bozovic, Phys. Rev. B **42**, 1969 (1990).
[55] T. Timusk and D. B. Tanner, Physica C **169**, 425 (1990).
[56] I. Bozovic *et al.*, Phys. Rev. B **43**, 1169 (1991).
[57] T. Timusk *et al.*, Phys. Rev. Lett. **66**, 663 (1991).
[58] M. Shimada *et al.*, Physica C **193**, 353 (1992).
[59] S. Tajima *et al.*, Phys. Rev. B **48**, 16164 (1993).
[60] M. J. Holcomb, J. P. Collman, and W. A. Little, Phys. Rev. Lett. **73**, 2360 (1994).
[61] D. C. Mattis and J. Bardeen, Phys. Rev. **111**, 412 (1958).
[62] W. Y. Lee *et al.*, J. Appl. Phys. **70**, 3952 (1991).
[63] $Tl_2Ba_2CaCu_2O_8$ thin film manufactured by Dupont Superconductivity, Central Research and Development, Wilmington, DE 19880-0304.
[64] A. E. Manzi and L. H. Luo, Physica C **185**, 2445 (1991).
[65] M. P. Siegal *et al.*, J. Mater. Res. **7**, 2658 (1992).
[66] M. J. Holcomb, J. P. Collman, and W. A. Little, Rev. Sci. Instrum. **64**, 1867 (1993).
[67] M. Cardona, in *Solid State Physics: Advances in Research and Applications*, edited by F. Seitz, D. Turnbull, and H. Ehrenreich (Academic, New York, 1960), Vol. 11, p. 117.
[68] LTMP system, Model R2400, manufactured by MMR technologies, Inc., 1400 N. Shoreline Blvd., Mt. View, CA 94043.
[69] SR810 lock-in amplifier, manufactured by Standford Research Systems, Inc., 1290-D Reamwood Ave., Sunnyvale, CA 94089.
[70] B. Batz, in *Semiconductors and Semimetals; Modulation Techniques*, edited by R. K. Willardson and A. C. Beer (Academic, New York, 1972), Vol. 9, p. 315.
[71] We note that there is a typographical error in the reflectance expression on p. 329 of Ref. 63.
[72] J. Ruvalds and A. Virosztek, Phys. Rev. B **43**, 5498 (1991).
[73] C. M. Varma, Int. J. Mod. Phys. B **3**, 2083 (1989).
[74] C. M. Varma *et al.*, Phys. Rev. Lett. **63**, 1996 (1989).
[75] E. J. Nicol and J. P. Carbotte, in *Studies of High Temperature Superconductors*, edited by A. Narlikar (Nova Science, New York, 1993), Vol. 11, p. 225.
[76] D. E. Aspnes and M. K. Kelly, IEEE J. Quantum Electron. **25**, 2378 (1989).
[77] T. Yamamoto *et al.*, Jpn. J. Appl. Phys. **31**, L327 (1992).
[78] S. Uchida, Physica (Amsterdam) **185–189C**, 28 (1991).
[79] H. You *et al.*, Phys. Rev. B **43**, 3660 (1989).
[80] We find that the inclusion of an ω^2 term in the optical scattering rate does not adequately describe the reflectance spectra of these materials.
[81] H. You *et al.*, Phys. Rev. B **38**, 9213 (1988).
[82] C. Meingast *et al.*, Phys. Rev. B **41**, 11299 (1990).
[83] Y. Ono and S. Narita, Jpn. J. Appl. Phys **31**, L224 (1992).

[84] M. Okaji *et al.*, Cryogenics **34**, 163 (1994).
[85] Z. J. Yang *et al.*, J. Supercond. **8**, 233 (1995).
[86] M. J. Holcomb (unpublished).
[87] N. W. Ashcroft and N. D. Mermin, in *Solid State Physics* (Saunders, Philadelphia, 1976), Chap. 1, p. 16.
[88] We use, for these simulations, the best-fit optical parameters obtained from our work. These values are shown in the T1-2223 section of Table IV.
[89] We do not present the temperature-dependent results for YBCO because of the poor quality of the theoretical fit.